Antenna Laboratory Report No. 69-10

RADIATION FROM AN OPEN-ENDED WAVEGUIDE INTO AN INHOMOGENEOUSLY FILLED SPACE

by

R. J. Kostelnicek and R. Mittra

Scientific Report No. 12

July 1969

Sponsored by
National Aeronautics and Space Administration
NGR-14-005-009

Antenna Laboratory
Department of Electrical Engineering
Engineering Experiment Station
University of Illinois
Urbana, Illinois 61801

Antenna Laboratory Report No. 69-10

RADIATION FROM AN OPEN-ENDED WAVEGUIDE INTO AN INHOMOGENEOUSLY FILLED SPACE

by

R. J. Kostelnicek and R. Mittra

Scientific Report No. 12

July 1969

Sponsored by
National Aeronautics and Space Administration
NGR-14-005-009

Antenna Laboratory
Department of Electrical Engineering
Engineering Experiment Station
University of Illinois
Urbana, Illinois 61801

ABSTRACT

An analytic solution to the problem of radiation from an open-ended parallel-plate waveguide into a dielectric or plasma slab is obtained. The electromagnetic fields are formulated in terms of a discrete mode spectrum inside the waveguide and continuous mode spectra in the open regions. Mode matching at the waveguide aperture plane leads to a singular integral equation. A solution of this equation allows the determination of the fields throughout the whole of space. However, this equation is not solved directly, but instead, an auxiliary integral equation is formed from the original equation by employing the known exact solution of the canonical problem, viz., radiation from an open-ended waveguide into free-space. The auxiliary equation has the advantage that it may be solved exactly in an asymptotic sense. This asymptotic solution demonstrates that the correct edge condition is satisfied. Standard numerical techniques are employed, and results giving the fields and distribution of scattered power for a TEM incident mode are presented.

Solutions for other problems are also formulated, viz., the flanged waveguide and a guide radiating into a reflecting screen. These problems may also be solved when the geometry is circular. Furthermore, the edge condition is also shown to be satisfied in circular geometry.

ACKNOWLEDGEMENT

The author acknowledges the financial aid given him by the National Science Foundation's Traineeship Program. Also a portion of the computer time was financed by the National Aeronautics and Space Administration under Contract Number NGR 14-005-009.

TABLE OF CONTENTS

LIST OF TABLES

LIST OF FIGURES

Figure | Page

1. INTRODUCTION

Exact solutions can be found for certain open-region boundary value problems in which the geometry can be separated into several distinct semi-infinite regions. For example, an open-ended parallel-plate waveguide radiating into a homogeneous space has been solved by Noble (1958) using the Weiner-Hopf technique and by Mittra and Bates (1965) employing an extension of the function-theoretic technique to open-regions. Recently, problems in which one of the regions is modified have also been found solvable. Bates and Mittra (1967), using the Weiner-Hopf technique, have found an analytic solution for the problem where a dielectric or plasma slab is excited by a semi-infinite waveguide (cf. Figure 1). An important characteristic of this problem is that the medium filling the open-region is non-uniform in the transverse direction, while the complete geometry is longitudinally uniform. When the geometry is non-uniform in the longitudinal direction, a class of boundary value problems results for which the Weiner-Hopf technique is no longer directly applicable. Figure 2 shows a longitudinally non-uniform problem, i.e., a semi-infinite parallel-plate waveguide radiating through a dielectric or plasma slab. The purpose of this work is to present a method based on the function-theoretic technique which is useful in attacking problems which have longitudinal non-uniformities.

Formulation of a problem by the function-theoretic technique is typically accomplished by employing the characteristic or normal modes in each region. Such a modal representation can be used to advantage when there is a longitudinal inhomogeneity within an individual region. This applies to stratified media as well. Such regional non-uniformities can be taken into account by the application of conventional mode-matching

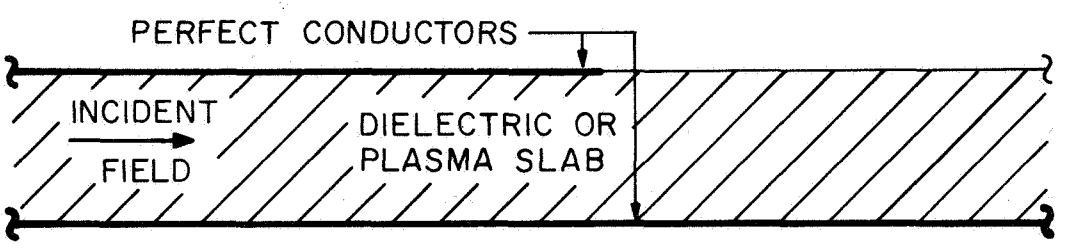

Figure 1. A longitudinally uniform open-region problem.

procedures at the interfaces between the various layers or subregions. An application of the continuity conditions at the aperture-plane of the waveguide, leads to an integral equation, which is an extended form of the corresponding equation for the unmodified geometry. An exact solution of this equation for the canonical problem, i.e., for the unmodified geometry, is available (Mittra and Bates, 1965) and is used in the construction of the solution of the problem shown in Figure 2.

A function $F(\omega)$ of a complex variable ω is constructed having a certain pole-zero structure and specified branch singularities. Certain manipulations with this function in the complex plane yield an integral equation which is then compared to the one obtained by mode-matching. By choosing a particular form for $F(\omega)$, together with the above comparison, an auxiliary integral equation is formed. This auxiliary equation may be solved instead of the original integral equation.

There are two definite advantages gained by employing the auxiliary integral equation. These advantages are: (1) The auxiliary equation is in a more efficient form for numerical solution than is the original integral equation. (2) An exact solution in the asymptotic sense of the auxiliary equation is possible. It is this asymptotic behavior which demonstrates that the correct edge condition is indeed satisfied (Meixner, 1954). It is often difficult if not impossible to prove the satisfaction of this condition when alternative methods are employed in constructing a solution.

2. RADIATION FROM AN OPEN-ENDED PARALLEL-PLATE WAVEGUIDE INTO AN INHOMOGENEOUSLY FILLED SPACE

2.1 Formulation of the Problem

Consider an open-ended parallel-plate waveguide radiating into an open-region which is partitioned by a dielectric slab. The geometry of this structure is shown in Figure 2. The waveguide is excited from the left by a single TEM or TM_{po} mode ($p = 1,2,....$) of unit amplitude in region B. The space surrounding the guide is divided into four regions: A, C, D, and E. A right-hand Cartesian coordinate system is placed at the guide aperture with the pertinent dimensions given by b, the guide half-width; ℓ, the guide-aperture separation; and t, the slab half-width. The relative permittivity of region A is given by κ while that of the remaining space is taken as unity.

A solution of the source-free Maxwell's equations for this geometry leads to a discrete eigenmode expansion of the electromagnetic fields in region B and transform representations in terms of the continuous mode spectra in the remaining open-regions. The transverse fields are matched at each of the regional interfaces, and the resulting equations are manipulated in order to yield expressions for the mode and spectral weight coefficients. These coefficients are then explicitly solved for by an appropriate modification of the function-theoretic technique. This technique, in its original form, was first applied to closed waveguide problems by Hurd and Gruenberg (1954) and to open periodic structures by Berz (1951) and Whitehead (1951). These early works yielded infinite matrix equations, the elements of which were functions of the longitudinal wave numbers and mode coefficients for the various regions. Mittra and Bates (1965) extended the function-theoretic technique to an open-region

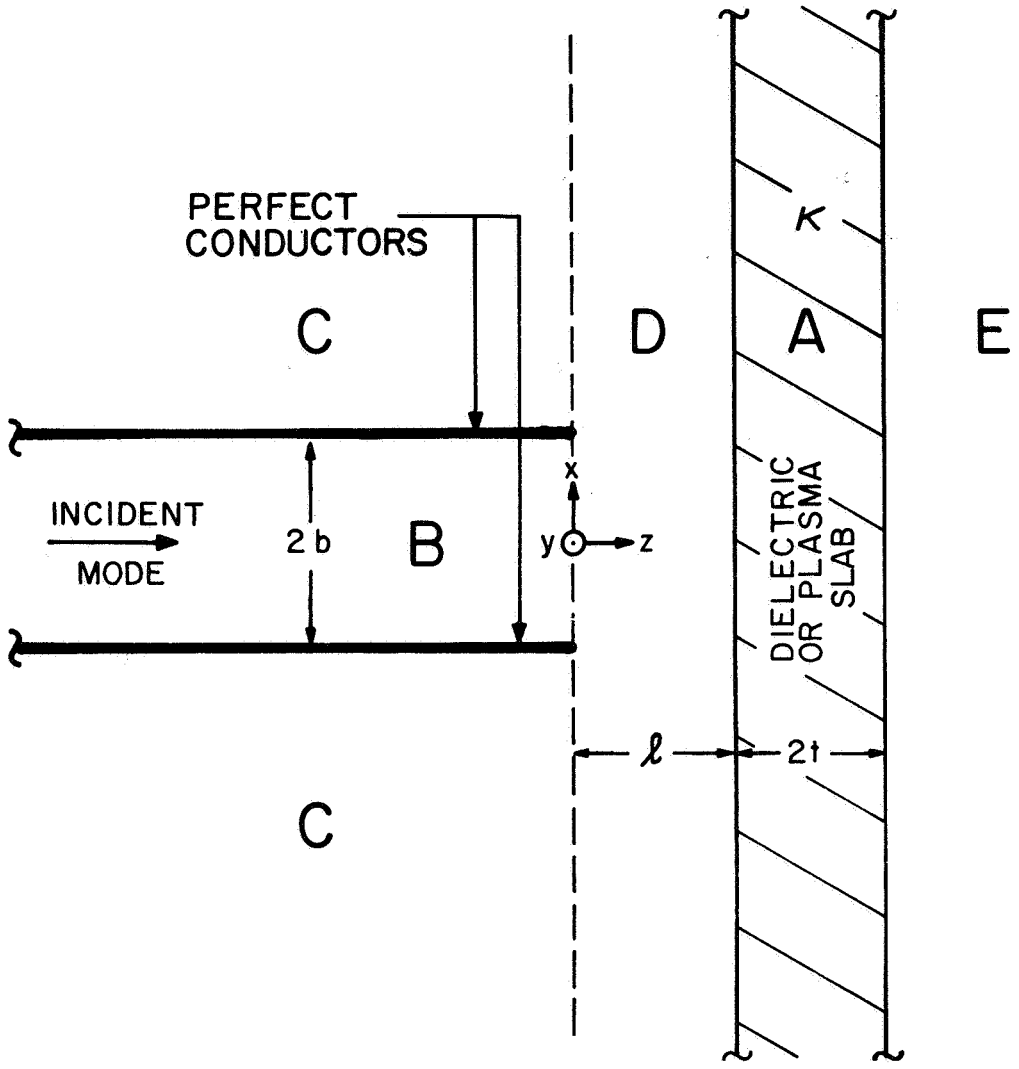

Figure 2. The radiating structure.

problem by employing a limit process to the associated closed-region problem. Due to the continuous nature of the eigenspectrum in the open-regions, an integral equation results corresponding to the infinite matrix equation for the associated closed-region problem. For the modified problem of Figure 2, an extended version of this integral equation is obtained, which can be transformed into a matrix equation by the usual numerical techniques.

The geometry of Figure 2, being y-independent and x-symmetric, scatters only TEM and TM type waves with respect to the z-coordinate. The total magnetic intensity $\Phi = H_y$ in each region is represented as follows:

$$\Phi_A = \frac{1}{2}\int_\sigma \left[A_1(\alpha)\cosh[\tau(z-\ell-t)] + A_2(\alpha)\sinh[\tau(z-\ell-t)]\right]\exp(-j\alpha x)\,d\alpha,$$

$$\ell \le z \le \ell + 2t, \qquad (2.1)$$

$$\Phi_B = \cos\left(\frac{p\pi x}{b}\right)\exp(-\beta_p z) + \sum_{s=o}^{\infty}\left[B_s\cos\left(\frac{s\pi x}{b}\right)\exp(\beta_s z)\right],$$

$$|x| \le b,\ z \le 0, \qquad (2.2)$$

$$\Phi_C = \frac{1}{2}\int_\sigma C(\gamma)\exp(\eta z)\exp[-j\gamma(x-b)]\,d\gamma,$$

$$x \ge b,\ z \le 0, \qquad (2.3a)$$

$$\Phi_C = \frac{1}{2}\int_\sigma C(\gamma)\exp(\eta z)\exp[-j\gamma(x+b)]\,d\gamma,$$

$$x \le -b,\ z \le 0, \qquad (2.3b)$$

$$\Phi_D = \frac{1}{2}\int_\sigma \left[D^+(\alpha)\ \exp(-\xi z) + D^-(\alpha)\ \exp(\xi z)\right]\ \exp(-j\alpha x)\ d\alpha,$$

$$0 \le z \le \ell, \qquad (2.4)$$

and

$$\Phi_E = \frac{1}{2}\int_\sigma E(\alpha)\ \exp[-\xi(z-\ell-2t)]\ \exp(-j\alpha x)\ d\alpha,$$

$$\ell + 2t \le z. \qquad (2.5)$$

The mode coefficients are given by B_s, $(s = 0,1,2...)$, in region B, and the spectral weight functions by $A_1(\alpha)$, $A_2(\alpha)$, $C(\gamma)$, $D^+(\alpha)$, $D^-(\alpha)$ and $E(\alpha)$ in their respective open-regions. The fields have a traveling wave representation in each region except A, where the representation is in terms of even and odd modes with respect to the z-coordinate. This is a convenient representation for region A when there are surface modes present within the slab. The variables of integration α and γ lie on the path σ shown in Figure 3. Use of the $\exp(j\omega t)$ time convention requires that the following function branches be employed in order to yield outgoing waves:

$$\xi = \sqrt{\alpha^2 - k_o^2} = j\sqrt{k_o^2 - \alpha^2} \qquad (2.6a)$$

$$\eta = \sqrt{\gamma^2 - k_o^2} = j\sqrt{k_o^2 - \gamma^2} \qquad (2.6b)$$

$$\tau = \sqrt{\alpha^2 - \kappa\, k_o^2} = j\sqrt{\kappa\, k_o^2 - \alpha^2} \qquad (2.7)$$

and

$$\beta_s = \sqrt{\left(\frac{s\pi}{b}\right)^2 - k_o^2} = j\sqrt{k_o^2 - \left(\frac{s\pi}{b}\right)^2}\ , \quad (s = 0,1,2,....). \qquad (2.8)$$

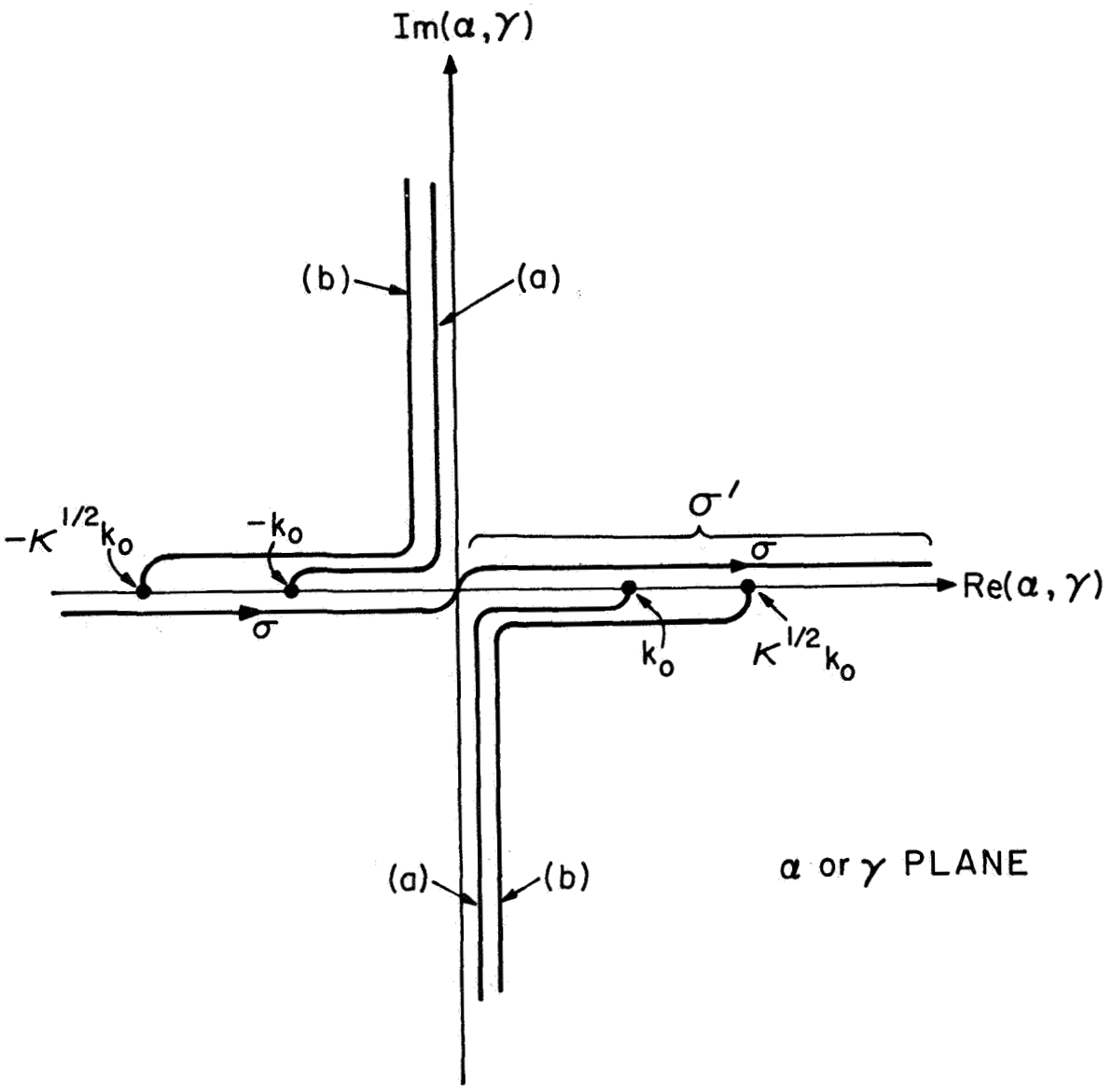

Figure 3. The path σ and the branch cuts for (a) $\xi(\alpha)$ and $\eta(\gamma)$, and (b) $\tau(\alpha)$ in the complex or α or γ-plane.

The free-space propagation constant is given by $k_o = \omega\sqrt{\mu_o \varepsilon_o}$, where ω is the angular frequency and μ_o and ε_o are respectively the permeability and permittivity of free-space. The branch cuts for (2.5) through (2.8) are shown in Figure 3 for κ-real and greater than unity. The remaining components of the electric field are obtained from the following relationships:

$$E_x = (j\omega\varepsilon_o\varepsilon_r)^{-1} \frac{\partial \Phi}{\partial z} \tag{2.9}$$

and

$$E_z = -(j\omega\varepsilon_o\varepsilon_r)^{-1} \frac{\partial \Phi}{\partial x} \quad , \tag{2.10}$$

where $\varepsilon_r = \kappa$ in region A and unity throughout the remaining space.

2.2 Representation in the Spectral Domain

The first step toward obtaining the solution of (2.1) through (2.5) is to express the unknown mode and weight coefficients in terms of $E(\alpha)$, the weight coefficient for the forward open-region. The procedure is to enforce the continuity conditions of the transverse field components at the three regional interfaces. Continuity at z=0 gives

$$\left.\begin{aligned} \Phi_B(x,o) &= \Phi_D(x,o) \qquad (2.11) \\ \frac{\partial \Phi_B(x,o)}{\partial z} &= \frac{\partial \Phi_D(x,o)}{\partial z} \qquad (2.12) \end{aligned}\right\} |x| \leq b$$

and

$$\left.\begin{aligned} \Phi_C(x,o) &= \Phi_D(x,o) \\ \frac{\partial \Phi_C(x,o)}{\partial z} &= \frac{\partial \Phi_D(x,o)}{\partial z} \end{aligned}\right\} \quad |x| \geq b \qquad (2.13)$$

$$(2.14)$$

Similarly, at $z = \ell$ we obtain

$$\Phi_D(x,\ell) = \Phi_A(x,\ell) \qquad (2.15)$$

$$\frac{\partial \Phi_D(x,\ell)}{\partial z} = \kappa^{-1} \frac{\partial \Phi_A(x,\ell)}{\partial z} , \qquad (2.16)$$

while at $z = \ell + 2t$ we have

$$\Phi_A(x,\ell+2t) = \Phi_E(x,\ell+2t) \qquad (2.17)$$

and

$$\kappa^{-1} \frac{\partial \Phi_A(x,\ell+2t)}{\partial z} = \frac{\partial \Phi_E(x,\ell+2t)}{\partial z} . \qquad (2.18)$$

Combining (2.17) and (2.18) yields the expressions for the even and odd spectral weight functions in region A

$$A_1(\alpha) = E(\alpha) \left[\cosh(\tau t) + \frac{\kappa\xi}{\tau} \sinh(\tau t)\right] \qquad (2.19)$$

and

$$A_2(\alpha) = E(\alpha) \left[\sinh(\tau t) + \frac{\kappa\xi}{\tau} \cosh(\tau t)\right]. \qquad (2.20)$$

Similarly, a combination of (2.15), (2.16), (2.19), and (2.20) gives the forward and backward traveling wave spectral weight functions in region D

$$D^{+}(\alpha) = E(\alpha)\, R'(\alpha) \tag{2.21}$$

and

$$D^{-}(\alpha) = E(\alpha)\, Q'(\alpha)\ , \tag{2.22}$$

where $R'(\alpha) = R(\alpha)\exp(\xi\ell)$ and $Q'(\alpha) = Q(\alpha)\exp(-\xi\ell)$, with

$$R(\alpha) = \cosh(2\tau t) + \frac{1}{2}\left[\frac{\kappa\xi}{\tau} + \frac{\tau}{\kappa\xi}\right]\sinh(2\tau t) \tag{2.23}$$

and

$$Q(\alpha) = \frac{1}{2}\left[\frac{\kappa\xi}{\tau} - \frac{\tau}{\kappa\xi}\right]\sinh(2\tau t)\ . \tag{2.24}$$

The above procedure, used to obtain expressions for the spectral weight functions in the regions lying between the guide aperture and the forward open-region, is not limited only to problems having two intermediate regions. One can express the weight functions in each region of an n-layered medium in terms of the corresponding function in the far-forward region. This procedure is similar to that of determining the voltage along each segment of a cascade of transmission lines, each portion having a different characteristic impedance, in terms of the voltage at the line's termination.

Fourier analyzing (2.11) and (2.12), i.e., multiplying each side of these relationships by $\cos(m\pi x/b)$, (m=0,1,....), and integrating with respect to x from -b to b, together with the relationships (2.21) and (2.22), yields

$$(-1)^p\ b\ (1+\delta_p^o)\ \delta_m^p + (-1)^m\ b\ B_m\ (1+\delta_m^o) =$$

$$\int_\sigma E'(\alpha) \left[\frac{R'(\alpha) + Q'(\alpha)}{\xi^2-\beta_m^2} \right] d\alpha \qquad (2.25)$$

and

$$(-1)^p\ b\ \beta_p(1+\delta_p^o)\ \delta_m^p - (-1)^m b\ \beta_m B_m\ (1+\delta_m^o) = \int_\sigma \xi\ E'(\alpha) \left[\frac{R'(\alpha) - Q'(\alpha)}{\xi^2-\beta_m^2} \right] d\alpha, \qquad (2.26)$$

where $E'(\alpha) = \alpha \sin(\alpha b)\ E(\alpha)$ and δ_i^j is the Kronecker delta defined by

$$\delta_i^j = \left\{ \begin{array}{l} 0, \text{ if } i \neq j \\ \\ 1, \text{ if } i = j \end{array} \right\}. \qquad (2.27)$$

The integrands of (2.25) and (2.26) have poles at $\xi = \pm\ \beta_m$ or equivalently when $\alpha = \pm\ m\pi/b$. These poles are cancelled by the corresponding zeros of $\sin(\alpha b)$, which is a factor of $E'(\alpha)$. Due to this pole-zero cancelation, the integrals of (2.25) and (2.26) need not be considered in the Cauchy principal value sense.

Multiplying (2.25) by β_m and first adding and then subtracting it from (2.26) yields

$$(-1)^p\ b\ \beta_p(1+\delta_p^o)\ \delta_m^p = \int_{\sigma'} E'(\alpha) \left[\frac{R'(\alpha)}{\xi-\beta_m} - \frac{Q'(\alpha)}{\xi+\beta_m} \right] d\alpha \qquad (2.28)$$

and

$$-\ (-1)^m\ b\ \beta_m B_m(1+\delta_m^o) = \int_{\sigma'} E'(\alpha) \left[\frac{R'(\alpha)}{\xi+\beta_m} - \frac{Q'(\alpha)}{\xi-\beta_m} \right] d\alpha\ . \qquad (2.29)$$

Note that the path σ employed in all integrations previous to (2.28) has been reduced to σ' in (2.28) and (2.29). This new path is identical to that portion of σ which extends from zero to infinity and lies entirely in the upper-half α-plane (cf. Figure 3). Such a reduction is carried out by requiring $E(\alpha)$ to be a symmetric function of α, the remaining part of the integrand being obviously symmetric.

Multiplying (2.13) by $\exp[j\gamma(x-b)]$ and integrating with respect to x from b to ∞, and repeating the same process with a multiplier $\exp[j\gamma(x+b)]$ and integrating from $-\infty$ to-b yields

$$\pi\, C(\gamma) = \pi\, E(\gamma)\, [R'(\gamma) + Q'(\gamma)] \cos(\gamma b)$$

$$- \text{P.V.} \int_{\sigma} E'(\alpha) \left[\frac{R'(\alpha) + Q'(\alpha)}{\xi^2 - \eta^2} \right] d\alpha \qquad (2.30)$$

and

$$\pi\, \eta\, C(\gamma) = -\pi\, \eta\, E(\gamma)\, [R'(\gamma) - Q'(\gamma)] \cos(\gamma b)$$

$$+ \text{P.V.} \int_{\sigma} E'(\alpha) \xi \left[\frac{R'(\alpha) - Q'(\alpha)}{\xi^2 - \eta^2} \right] d\alpha \,. \qquad (2.31)$$

Due to the continuous nature of η, a cancelling of the poles at $\xi = \pm\, \eta$ is not found except when $\eta = \pm\, \beta_m$. Therefore, the integrals in (2.30) and (2.31) are written as the Cauchy principal value type.

Combining (2.30) and (2.31), as was done in obtaining (2.28) and (2.29), gives

$$\pi\, \eta\, E(\gamma) R'(\gamma) \cos(\gamma b) = \text{P.V.} \int_{\sigma'} E'(\alpha) \left[\frac{R'(\alpha)}{\xi - \eta} - \frac{Q'(\alpha)}{\xi + \eta} \right] d\alpha \qquad (2.32)$$

and

$$\pi\,\eta\,C(\gamma) - \pi\,\eta\,E(\gamma)\,Q'(\gamma)\cos(\gamma b) =$$

$$\text{P.V.}\int_{\sigma'} E'(\alpha)\left[\frac{R'(\alpha)}{\xi+\eta} - \frac{Q'(\alpha)}{\xi-\eta}\right] d\alpha\ . \qquad (2.33)$$

Equations (2.29) and (2.33) express the two remaining unknowns, viz., B_s and $C(\gamma)$, in terms of $E(\alpha)$. Comparing (2.28) with (2.32), i.e., when $\eta = \beta_m$, we obtain the values of $E(\alpha)$ at a countable-infinite number of points

$$E(s\pi/b) = \left\{ \begin{array}{ll} b\ (1+\delta_p^o)\left[\pi R'(p\pi/b)\right]^{-1} & ;\ s = p \\ \\ 0 & ;\ s \neq p \end{array} \right\}. \qquad (2.34)$$

Equation (2.32) together with (2.34) represents a homogeneous integral equation for $E(\alpha)$ with prescribed function values at particular values of α. In the following section a method is presented to solve this integral equation based on an extension of the function-theoretic technique for open-regions.

2.3 Modification of the Function-Theoretic Technique

As stated in the introduction, a closed-form solution to the problem associated with the geometry of Figure 2, but with the dielectric or plasma slab removed (hereafter called the canonical problem), has been obtained. When the slab is inserted, one finds that by employing a suitably modified version of the function-theoretic technique, an analytic solution is still possible. However, the solution is no longer in a

closed-form, but is most easily obtained from the solution of an auxiliary integral equation.

2.3.1 Solution in the Spectral Domain

Consider a function $F(\omega)$ of a complex variable ω, which is factored as follows:

$$F(\omega) = F_1(\omega)\ T(\omega)\ . \tag{2.35}$$

The factor $F_1(\omega)$ is that function which one employs in the solution of the canonical problem (Mittra and Bates, 1965) by the function-theoretic technique, and is given by

$$F_1(\omega) = K\ \Pi(\omega,\beta)\ N(\omega)\ (\omega-\beta_o) \tag{2.36}$$

The constant K is a normalization factor which depends upon the amplitude of the incident waveguide mode.

$$\Pi(\omega,\beta) = \prod_{s=1}^{\infty}\left[\left(1 - \frac{\omega}{\beta_s}\right)\ \exp(\omega/\beta_s)\right] \tag{2.37}$$

is an absolutely convergent infinite product expansion, and

$$N(\omega) = \exp\left[\frac{b\omega}{\pi}\left[1-C_e + \ln\left(\frac{2\pi}{k_o b}\right)\right] - j\ \frac{b\omega}{2} + \right.$$

$$\left.\frac{b}{\pi}\sqrt{\omega^2+k_o^2}\ \ln\left(\frac{\omega-\sqrt{\omega^2+k_o^2}}{-j\ k_o}\right)\right] \tag{2.38}$$

is obtained from the limit function of the ratio of two infinite product expansions associated with regions C and D in the canonical closed-region

problem as the outer guide is made infinitely wide (cf. Section 2.3.2). The constant C_e in (2.38) is equal to Euler's constant.

For large values of ω, the canonical function $F_1(\omega)$ decays exponentially in the upper half ω-plane and decreases algebraically as $|\omega|^{-1/2}$ in the lower half-plane. Furthermore, $F_1(\omega)$ has a branch point at $\omega = \beta_o$ and a branch singularity, shown in Figure 4, due to $N(\omega)$. As will become apparent in the sequel, the composite function $F(\omega)$ must have a simple pole at $\omega = \beta_p$, the propagation constant for the incident guide mode, and a branch point at $\omega = -\beta_o$. Therefore, we require $T(\omega)$ to possess these added singularities with a branch cut along the reflection of the cut for $F_1(\omega)$ (cf. Figure 4.). The edge condition (Meixner, 1954) requires that $F(\omega) \to O(\omega^{-1/2-\nu})$ as $|\omega| \to \infty$, $\arg(\omega) = -\pi$, and therefore, it is stipulated that $T(\omega) \to O(\omega^{-\nu})$, where

$$\nu = \left\{ \begin{array}{ll} 1-\max\left(\frac{1}{\pi}\arcsin\left[\frac{\kappa-1}{\kappa+1}\right] , 0\right) & ; \ell = 0 \\ 1 & ; \ell > 0 \end{array} \right\} . \qquad (2.39)$$

The branch of arcsin is chosen as follows:

$$-\frac{\pi}{2} \leq \arcsin(\theta) \leq \frac{\pi}{2} \; ; \; -1 \leq \theta \leq 1 \; . \qquad (2.40)$$

The integral equation (2.32) for the weight function $E(\alpha)$ can now be solved. Integration of the function $F(\omega)/(\omega-\eta)$ along the path Σ (cf. Figure 4), with η placed directly on the branch singularity, yields

$$\frac{1}{2\pi j}\int_{\Sigma}\frac{F(\omega)}{\omega-\eta}\,d\omega = P.V.\,\frac{1}{2\pi j}\int_{\sigma_1+\sigma_2}\frac{F(\omega)}{\omega-\eta}\,d\omega + \frac{1}{2\pi j}\int_{\sigma_3+\sigma_4}\frac{F(\omega)}{\omega-\eta}\,d\omega$$

$$-\frac{1}{2}F(\eta|_{\sigma_1}) - \frac{1}{2}F(\eta|_{\sigma_2}) = 0 \; . \qquad (2.41)$$

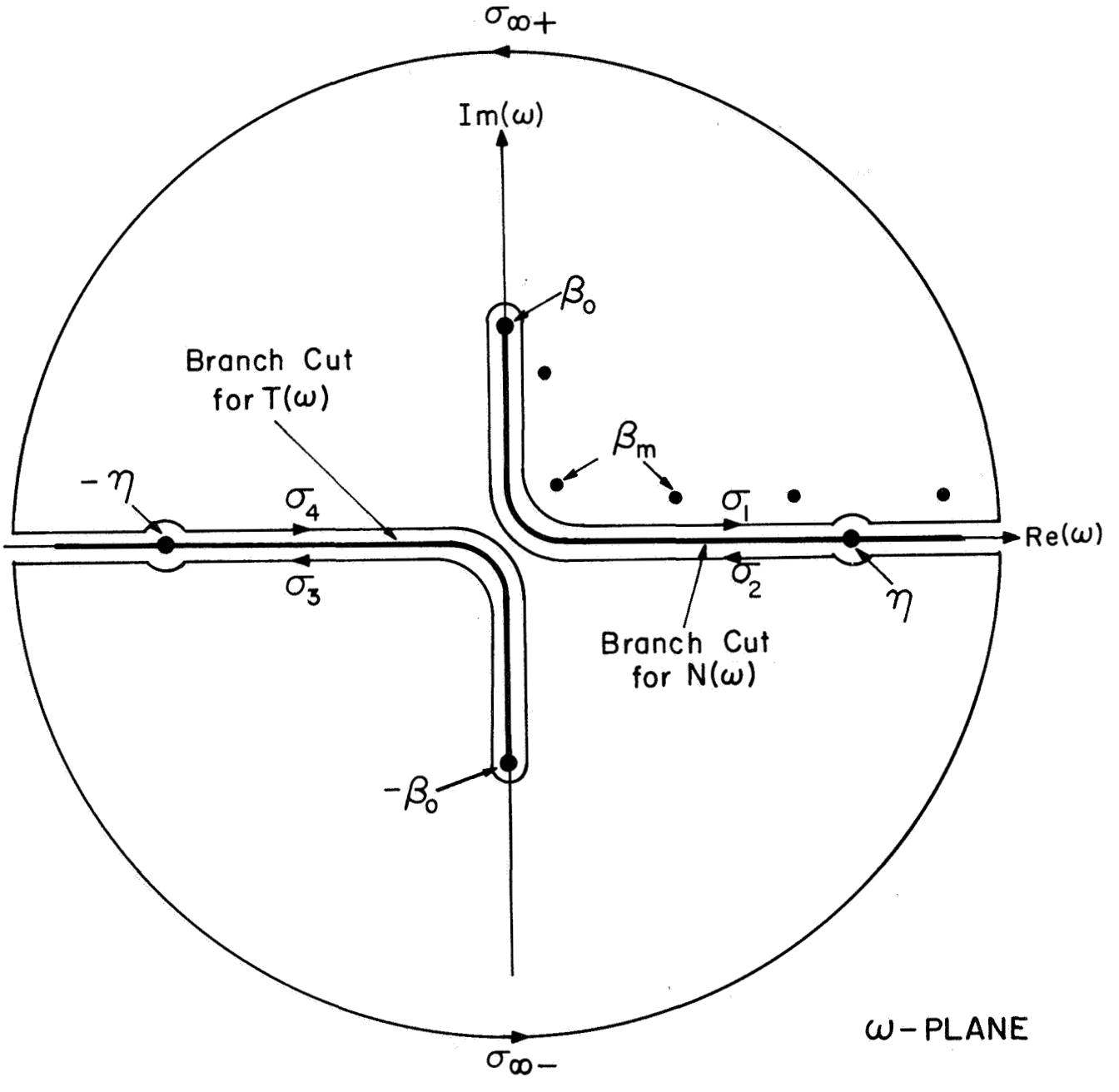

$$\sum = (\sigma_1+\sigma_2+\sigma_3+\sigma_4+\sigma_{\infty+}+\sigma_{\infty-})$$

Figure 4. The contour Σ in the complex ω-plane.

The integrals along the contours $\sigma_{\infty+}$ and $\sigma_{\infty-}$ are zero in (2.41) due to the exponential decay and algebraic decrease respectively of the integrands along these paths as $|\omega| \to \infty$. The integrals along the paths σ_1 and σ_2 are interpreted as being of the Cauchy principal value type. Employing the relationship

$$N(\omega\big|_{\sigma_2}) = N(\omega\big|_{\sigma_1}) \exp(-2jb\sqrt{\omega^2+k_o^2}), \tag{2.42}$$

which expresses the discontinuity in $N(\omega)$ across the branch cut, and by transforming the integral along σ_3 and σ_4 into a single integral along σ_1 via the transformation of variable $\omega \to -\omega$, (2.41) is reduced to the following form:

$$F(\eta\big|_{\sigma_1}) \exp(-j\gamma b) \cos(\gamma b) = \text{P.V.} \int_{\sigma_1} \left[\frac{F(\omega\big|_{\sigma_1}) \left[1-\exp(-2jb\sqrt{\omega^2+k_o^2})\right]}{2\pi j\ (\omega-\eta)} \right.$$

$$\left. + \frac{F(-\omega\big|_{\sigma_3}) - F(-\omega\big|_{\sigma_4})}{2\pi j\ (\omega+\eta)} \right] d\omega \ . \tag{2.42}$$

The integral in (2.42) is next transformed into an integral along the path σ', which was employed in (2.32), via the transformation of variable $\omega = \xi$ and $d\omega = \alpha\ d\alpha/\xi$. The result is given by

$$F(\eta\big|_{\sigma_1}) \exp(-j\gamma b) \cos(\gamma b) = \text{P.V.} \int_{\sigma'} \left[\frac{\alpha\ F(\xi\big|_{\sigma_1}) \sin(\alpha b) \exp(-j\alpha b)}{\xi\ \pi\ (\xi-\eta)} \right.$$

$$\left. + \frac{\alpha\ [F(-\xi\big|_{\sigma_3})-F(-\xi\big|_{\sigma_4})]}{\xi\ 2\pi j\ (\xi+\eta)} \right] d\alpha \ . \tag{2.43}$$

A direct comparison of the integrands of (2.43) and (2.32) yields

$$E(\alpha) = \frac{F(\xi|_{\sigma_1}) \exp(-j\alpha b)}{R'(\alpha)\ \pi\ \xi} \tag{2.44}$$

and

$$E(\alpha) = -\frac{[F(-\xi|_{\sigma_3}) - F(-\xi|_{\sigma_4})]}{Q'(\alpha)\ 2\pi j\ \sin(\alpha b)\ \xi}\ . \tag{2.45}$$

A comparison of the non-integrated terms yields

$$F(\eta|_{\sigma_1})\ \cos(\gamma b)\ \exp(-jb\gamma) = \pi\ \eta\ E(\gamma)\ R'(\gamma)\ \cos(\gamma b)\ . \tag{2.46}$$

Equations (2.44) and (2.46) are identical when $\eta = \xi$ and $\gamma = \alpha$. This identity shows the self-consistency of the solution for $E(\alpha)$ as determined by (2.44) or (2.46). Furthermore, $E(\alpha)$, as obtained from (2.44), is seen to satisfy the conditions at $\alpha = (s\pi/b)$, given by (2.34). It is from the value of $E(\alpha)$ at $\alpha = (p\pi/b)$ that the normalization constant K employed in (2.36) is determined. With the aid of (2.34) and (2.38), K is then obtained from the relationship

$$F(\beta_p|_{\sigma_1}) = b\ \beta_p\ (-1)^p\ (1+\delta_p^o). \tag{2.47}$$

In order that (2.44) and (2.45) be consistent expressions for $E(\alpha)$ they are first equated to one another, then the factored form of $F(\omega)$ is substituted, and finally the results are rearranged in order to obtain

$$T(-\xi|_{\sigma_3}) - T(-\xi|_{\sigma_4}) = 2\pi j\ \lambda(\xi)\ T(\xi), \tag{2.48}$$

where $\lambda(\xi)$ is given by

$$\lambda(\xi) = - \frac{Q'(\alpha)\ F_1(\xi|_{\sigma_1})\ \sin(\alpha b)\ \exp(-j\alpha b)}{\pi\ R'(\alpha)\ F_1(-\xi|_{\sigma_3})} . \qquad (2.49)$$

Equation (2.48) represents an expression of the discontinuity in $T(-\xi)$ across the branch cut, as shown in Figure 4, in terms of the function value $T(\xi)$ at the reflection point ξ. In Section 2.4, (2.48) is transformed into the integral equation which was previously referred to as the auxiliary integral equation.

At this point, the problem is solved contingent upon the construction of $T(\omega)$. However, simpler expressions exist for the mode coefficients B_m and weight function $C(\gamma)$, than the integral representations given by (2.29) and (2.33). Integrating along the contour Σ with $-\beta_m$ replacing η in (2.41), together with the subsequent transformation of variable and a direct comparison of the result with (2.29), yields

$$B_m = - \frac{(-1)^m\ F(-\beta_m|_{\sigma_3})}{b\ \beta_m\ (1+\delta_m^o)} . \qquad (2.50)$$

The same process with η replaced by $-\eta$ yields

$$C(\gamma) = \frac{1}{\pi\eta} \left[F(-\eta|_{\sigma_3}) \frac{Q'(\gamma)}{R'(\gamma)} + F(\eta|_{\sigma_1}) \right] . \qquad (2.51)$$

Before continuing on to the solution of $T(\omega)$, we digress so that we may compare the solution just derived with that for the corresponding closed-region problem. This is done to gain some insight into the form of the auxiliary integral equation.

2.3.2 Comparison with the Closed-Region Problem

The closed-region geometry associated with the problem just solved, is shown in Figure 5. The outer guide now has a finite half-width given by a. In all of the regions, the fields are now represented by eigenmode expansions due to the discrete nature of the eigenvalue spectrum for closed-regions. The formulation of the problem follows closely that of Section 2.1, with the exception that all of the integrals are replaced by infinite summations, and the continuous propagation constants take on discrete values

$$\xi_s = \sqrt{\left(\frac{s\pi}{a}\right)^2 - k_o^2} \tag{2.52}$$

$$\tau_s = \sqrt{\left(\frac{s\pi}{a}\right)^2 - \kappa\, k_o^2} \tag{2.53}$$

and

$$\eta_s = \sqrt{\left(\frac{s\pi}{c}\right)^2 - k_o^2} \quad , \tag{2.54}$$

where $c = a - b$.

Mode matching in the plane of the small guide's aperture and subsequent manipulations of the resulting equations, yields a doubly-infinite set of matrix equations for the mode coefficients E_s. This set of equations is given by

$$(-1)^p\, b\, \beta_p\, (1+\delta_p^o)\, \delta_m^p = 2b\, \beta_o\, E_o\, R_o'\, \delta_m^o + \sum_{s=1}^{\infty} E_s' \left[\frac{R_s'}{\xi_s - \beta_m} - \frac{Q_s'}{\xi_s + \beta_m}\right] \tag{2.55a}$$

and

$$0 = 2c\, \eta_o\, E_o\, R_o\, \delta_m^o - \sum_{s=1}^{\infty} E_s' \left[\frac{R_s'}{\xi_s - \eta_m} - \frac{Q_s'}{\xi_s + \eta_m}\right], \tag{2.55b}$$

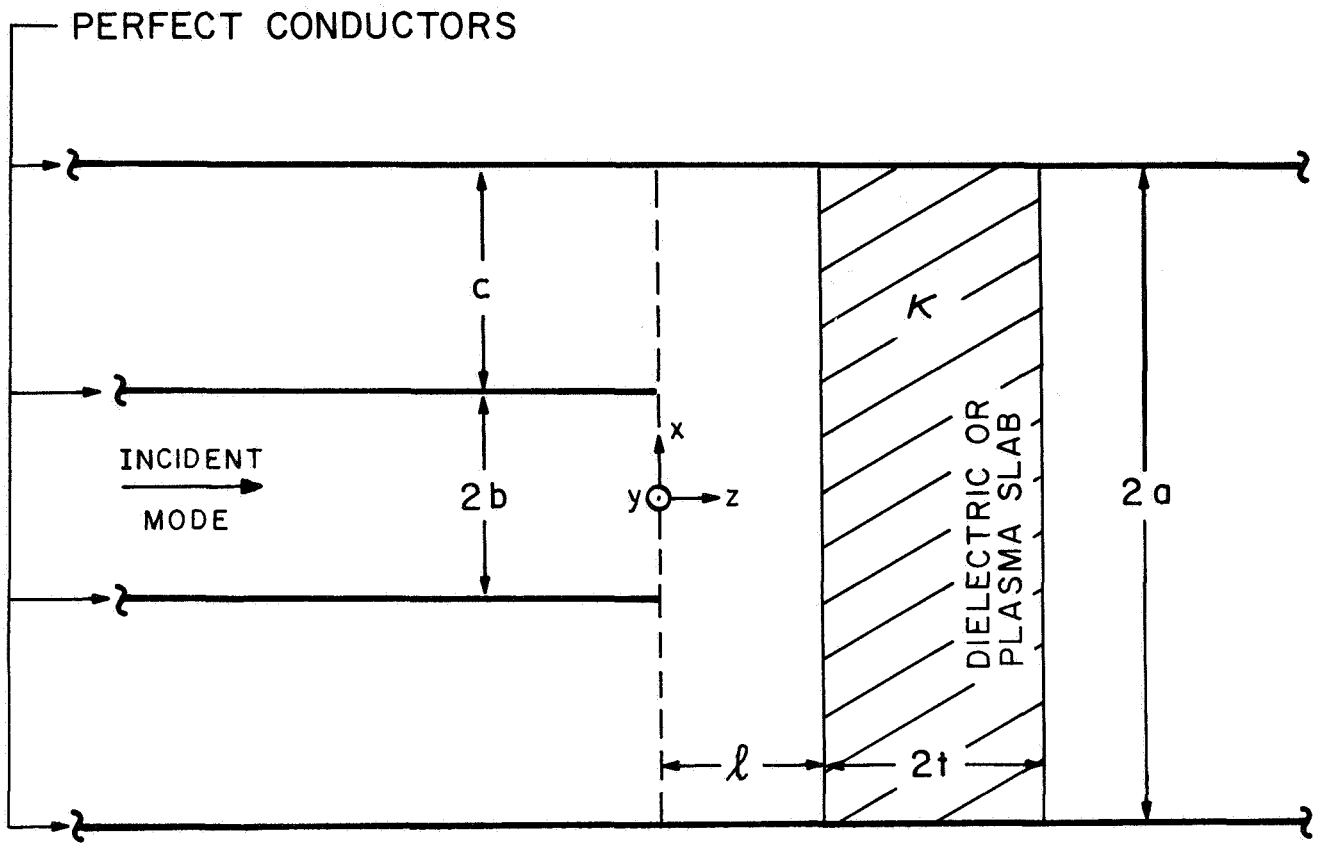

Figure 5. The closed region problem.

where

$$R'_s = R'\left(\frac{s\pi}{a}\right), \qquad Q'_s = Q'\left(\frac{s\pi}{a}\right), \qquad \text{and } E'_s = \left(\frac{s\pi}{a}\right) \sin\left(\frac{s\pi b}{a}\right) E_s.$$

In the infinite summation of (2.55b), it is assumed that $\xi_s \neq \eta_m$ for all values of s and m. This is equivalent to requiring that the ratio of the outer and inner guide half-widths, viz., a/b , is not a rational number. However, when this ratio is a rational number, we exclude from the summation in (2.55b) the q-th term when $\xi_s = \eta_q$, and add to the term outside the summation the limit of the s = q-th term as $s \to q$. The appropriate limit is given by

$$\lim_{s \to q} \left[\frac{E'_s R'_s}{\xi_s - \eta_q}\right] = - E_q R'_q \eta_q b \frac{c}{a} \cos(\gamma_q b), \tag{2.56}$$

where we have written $\gamma_q = (q\pi/c)$. When the outer guide becomes infinitely large, i.e., $c/a \to 1$, $a - c = b$, (2.56) becomes the term outside the integral in (2.32) for the corresponding open region-problem, viz., $-\pi\eta E(\gamma)R'(\gamma) \cos(\gamma b)$. Due to the continuous nature of the eigen-spectrum in the open region case, this non-integrated term is always present, since we are forced to let $\xi = \eta$ and $\alpha = \gamma$.

A solution of the doubly-infinite set of matrix equations is carried out by a modified version of the function-theoretic technique. The unmodified technique was employed by Hurd and Gruenberg (1954) for the solution of matrix equations associated with the bifurcated waveguide problem. A form for modifying the function-theoretic technique so that it can be employed to solve the bifurcated waveguide problem, with one of the interior regions modified was first presented by Mittra, Lee, and Vanblaricum (1968). In this form, the infinite product expansion

associated with the modified region was written as a new infinite product expansion containing a countable-infinite number of shifts in the zeros of the original expansion, i.e., shifts from the zeros associated with the unmodified problem. This zero-shift method is useful for closed region problems, but becomes awkward in the open-region case. The difficulty with the zero-shift formulation is that one cannot easily determine the limit function generated by the shifted infinite product expansions as the outer guide width becomes infinitely large. An alternative form for modifying the infinite product expansion is to employ an equivalent partial fraction expansion

$$\prod_{s=1}^{\infty}\left[\left(1-\frac{\omega}{\eta_s+\Delta_s}\right)\exp\left(\frac{\omega}{\eta_s+\Delta_s}\right)\right]=\Pi(\omega,\eta)\left[1+\omega\sum_{s=1}^{\infty}\frac{g_s}{\omega-\eta_s}\right]. \quad (2.57)$$

Equation (2.57) shows the expansion containing the unknown shifts Δ_s on the left, while an equivalent form is shown on the right. This equivalent form is written in terms of the unmodified expansion $\Pi(\omega,\eta)$ and the partial fraction expansion coefficients g_s. When the limit process is considered, i.e., $(a,c) \to \infty$ and $a - c = b$, it is found that the partial fraction expansion has an integral form for a limit function

$$\left[1+\omega\sum_{s=1}^{\infty}\frac{g_s}{\omega-\eta_s}\right]\to\left[1+\omega\int_{\sigma_1}\frac{g(z)\,dz}{\omega-\eta(z)}\right]. \quad (2.58)$$

The ratios of the infinite product expansion associated with regions C and D of Figure 5 are found to have the following limit function:

$$\lim_{\substack{a,c\to\infty\\ a-c=b}}\left[\frac{\Pi(\omega,\eta)}{\Pi(\omega,\xi)}\right]\to\bar{N}(\omega) . \quad (2.59)$$

The function $\overline{N}(\omega)$ is closely related to that given by (2.38). This relationship will be shown in Section 4. This function $\overline{N}(\omega)$ was originally obtained by the limiting process by Bates and Mittra (1965).

The solution of (2.55a) and (2.55b) for E_s by the function-theoretic technique, is accomplished by the construction of a meromorphic function $H(\omega)$. This function in a factored form is written

$$H(\omega) = H_1(\omega) \left[\frac{1}{\omega-\beta_p} + \sum_{s=1}^{\infty} \frac{g_s}{\omega+\xi_s} \right], \tag{2.60}$$

where $H_1(\omega)$ is that function employed in the solution of the canonical problem (Hurd & Gruenberg, 1954). Manipulations in the complex plane similar to those for the open-region problem (there is no branch singularity to circumvent in the contour integration) yield solutions for the various mode coefficients.

$$B_o = \frac{b}{a} \frac{Q_o'}{R_o'} \delta_p^o - \frac{H(-\beta_o)}{2b\ \beta_o} \tag{2.61}$$

$$B_s = -\frac{(-1)^s\ H(-\beta_s)}{b\ \beta_s}, \quad (s = 1,2,\ldots), \tag{2.62}$$

$$C_o = \frac{b}{a} \frac{Q_o'}{R_o'} \delta_p^o + \frac{H(-\eta_o)}{2c\ \eta_o} \tag{2.63}$$

$$C_s = \frac{H(-\eta_s)}{c\ \eta_s}, \quad (s = 1,2,\ldots), \tag{2.64}$$

and

$$E_o = \frac{b}{a} \frac{1}{R_o'} \delta_p^o \tag{2.65}$$

$$E_s = \frac{\text{residue } H(\omega = \xi_s)}{\left(\frac{s\pi}{a}\right) \sin\left(\frac{s\pi b}{a}\right)} \quad \frac{1}{R'_s} \quad , \ (s = 1,2,\ldots), \qquad (2.66)$$

$$E_s = -\frac{\text{residue } H(\omega = -\xi_s)}{\left(\frac{s\pi}{a}\right) \sin\left(\frac{s\pi b}{a}\right)} \quad \frac{1}{Q'_s} \quad , \ (s = 1,2,\ldots) \ . \qquad (2.67)$$

Elimination of E_s from (2.66) and (2.67) yields an infinite auxiliary matrix equation for the expansion coefficients

$$g_s = \lambda_s \left[\frac{1}{\zeta_s - \beta_p} + \sum_{m=1}^{\infty} \frac{g_m}{\zeta_s + \zeta_m} \right] , \qquad (s = 1,2,\ldots), \qquad (2.68)$$

where

$$\lambda_s = -\frac{Q'_s}{R'_s} \ \frac{\text{residue } H_1(\omega = \xi_s)}{H_1(-\xi_s)} \ . \qquad (2.69)$$

The normalization condition, which depends on the amplitude of the incident guide mode, is given by

$$H(\beta_p) = \left\{ \begin{array}{ll} \frac{2c}{a} \, b \, \beta_o & , \ p = o \\ (-1)^p \, b \, \beta_p & , \ p \neq o \end{array} \right\} . \qquad (2.70)$$

As the outer guide becomes infinitely wide, we expect (2.68) to become the auxiliary integral equation associated with the open-region problem. This is indeed the case, and the discussion in the following section will confirm this result.

2.4 Solution of the Auxiliary Integral Equation

In the preceeding section, we stated that in the limit as the outer guide half-width became infinite, that (2.68) would become an integral

equation for the unknown expansion coefficient g_t. To this end, we rewrite the partial fraction expansion

$$G(\omega) = \left[\frac{1}{\omega-\beta_p} + \sum_{m=1}^{\infty} \frac{g_m}{\omega+\xi_m}\right] \tag{2.71}$$

and the auxiliary matrix equation

$$g_s = \lambda_s \left[\frac{1}{\xi_s-\beta_p} + \sum_{m=1}^{\infty} \frac{g_m}{\xi_s+\xi_m}\right] . \tag{2.68}$$

As the outer guide recedes to infinite, we would expect

$$G(\omega) \rightarrow \left[\frac{1}{\omega-\beta_p} + \int_{\sigma_1} \frac{g(z)}{\omega+z}\, dz\right] \tag{2.72}$$

and

$$g(\omega) = \lambda(\omega) \left[\frac{1}{\omega-\beta_p} + \int_{\sigma_1} \frac{g(z)}{\omega+z}\, dz\right] . \tag{2.73}$$

A combination of (2.72) and (2.73) yields

$$g(\omega) = \lambda(\omega)\, G(\omega) \tag{2.74a}$$

and

$$G(\omega) = \left[\frac{1}{\omega-\beta_p} + \int_{\sigma_1} \frac{\lambda(z)\, G(z)}{\omega+z}\, dz\right] . \tag{2.74b}$$

Equation (2.74b) is an integral equation for $G(\omega)$ when ω is on the path σ_1. It can be shown that this expression is the auxiliary integral equation referred to in Section 2.3.2.

The expression for $G(\omega)$, given by (2.74b), has a branch singularity along the reflection of the path of integration. We evaluate $G(\omega)$ on each side of this branch cut and obtain

$$G(-\omega|_{\sigma_3}) = \frac{-1}{\omega+\beta_p} + j\pi\ \lambda(\omega)\ G(\omega|_{\sigma_1}) + P.V. \int_{\sigma_1} \frac{\lambda(z)\ G(z)}{z-\omega}\ dz \quad (2.75a)$$

and

$$G(-\omega|_{\sigma_4}) = \frac{-1}{\omega+\beta_p} - j\pi\ \lambda(\omega)\ G(\omega|_{\sigma_1}) + P.V. \int_{\sigma_1} \frac{\lambda(z)\ G(z)}{z-\omega}\ . \quad (2.75b)$$

Subtracting (2.75b) from (2.75a), gives an expression for the discontinuity in $G(\omega)$ across the branch singularity

$$G(-\omega|_{\sigma_3}) - G(-\omega|_{\sigma_4}) = 2\pi j\ \lambda(\omega)\ G(\omega|_{\sigma_1})\ . \quad (2.76a)$$

This process for obtaining the branch discontinuity for a singular integral is based on the use of the Plemelj formula (Muskheliskvili, 1964). A comparison of (2.76a) with (2.48) shows that if $G(\omega)$ is identified with $T(\omega)$, that (2.74b) is the required auxiliary integral equation

$$T(\omega) = \frac{1}{\omega-\beta_p} + \int_{\sigma_1} \frac{\lambda(z)\ T(z)}{\omega+z}\ . \quad (2.76b)$$

In the following section, (2.76b) will be transformed into a suitable form for numerical methods of solution.

2.4.1 Conversion to a Smooth Kernel

Close inspection of the partial kernel $\lambda(z)$ in equation (2.76b), reveals that the path σ_1 passes directly over the poles of $R^{-1}(z)$. It will be shown in Section 2.5 that there is at least one zero of $R(z)$ lying in the open interval $(k_o, \kappa^{1/2}k_o)$, when $\kappa > 1$ and real. These zeros of $R(z)$ correspond to TM-type surface modes within the dielectric slab. An attempt to solve for $T(\omega)$ on the path σ_1 will result in an integral of the Cauchy principal value type, which is in general, unsuitable for numerical methods of solution.

Equation (2.76b), as it presently stands, has a singular kernel. This equation is converted to one which has a "smooth" kernel by changing the path of integration to one on which the kernel is analytic. Such a path is shown in Figure 6 and is labeled by σ_1'. Equation (2.76b) then becomes

$$T(\omega) = \frac{1}{\omega-\beta_p} + \int_{\sigma_1'} \frac{\lambda(z)\, T(z)}{\omega+z}\, dz \qquad (2.77)$$

In continuously deforming the path from σ_1 to σ_1', no singularities of the integrand of (2.76b) are encountered, since the integrand is analytic in region S(cf. Figure 6). Using the Cauchy theorem, the integrals in (2.76b) and (2.77) give identical results for ω on the path σ_1.

Equation (2.77) is no longer applicable when ω is in region V of Figure 6. The effect of changing the path of integration from σ_1 to σ_1' is to shift the cut in the Rieman sheet for $T(\omega)$ from a position directly above the path σ_3 to one directly above σ_3' (cf. Figure 6). However, we may analytically continue the solution for $T(\omega)$ as given by (2.77) into region V by employing the relationship which describes the branch discontinuity, viz., equation (2.48). The correct result for

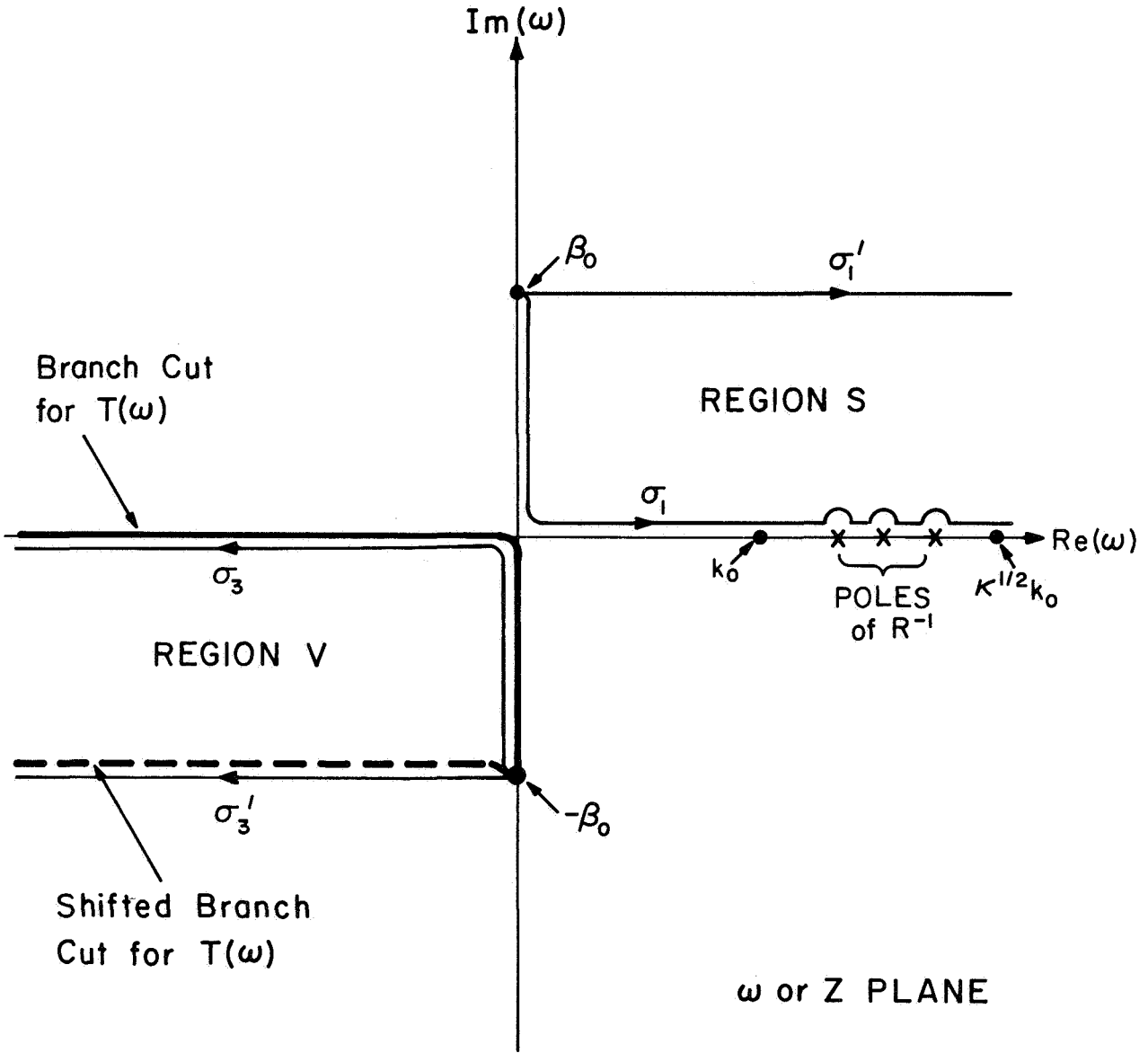

Figure 6. The integration paths for $T(\omega)$ and the region V of analytic continuation in the complex ω or z-plane.

$T(\omega)$, when ω is in region V, is given by

$$T(\omega) = 2\pi j\ \lambda(-\omega)\left[\frac{-1}{\omega+\beta_p} + \int_{\sigma_1'} \frac{\lambda(z)\ T(z)}{-\omega+z}\ dz\right] +$$

$$\left[\frac{1}{\omega-\beta_p} + \int_{\sigma_1'} \frac{\lambda(z)\ T(z)}{\omega+z}\right] dz \quad . \tag{2.78}$$

Equations (2.77) and (2.78) are in a convenient form for numerical computation. We first solve (2.77) for $T(\omega)$ on the path σ_1', and then substitute the proper values of ω on σ_1 and σ_3 into (2.77) and (2.78) respectively, to obtain $T(\omega|_{\sigma_1})$ and $T(-\omega|_{\sigma_3})$.

2.4.2 Satisfaction of the Edge Condition

In order that the solution obtained in Section 2.3 be acceptable, it must be demonstrated that the correct edge condition (Meixner, 1954) is satisfied at the guide edges, viz., ($x = \pm b$, $z=0$). Due to the manner in which $F(\omega)$ was factored in (2.35), it must be shown that $T(\omega) \to O[\omega^{-\nu}]$ as $|\omega| \to \infty$, where ν is given by (2.39). For large $|\omega|$, (2.76) can be written in the following asymptotic form:

$$T(\omega) \to \int_0^\infty \frac{\Lambda(z)\ T(z)}{\omega+z}\ dz + O\left[\frac{1}{\omega}\right] \quad , \tag{2.79}$$

where $\Lambda(z)$ is the asymptotic value of $\lambda(z)$, and is given by

$$\Lambda(z) = \lim_{z\to\infty}\left[\lambda(z)\right] = \left\{\begin{array}{ll} \frac{2}{\pi}\left[\frac{\kappa-1}{\kappa+1}\right]\ \sin^2(zb) & ;\ \ell = 0 \\ \\ O[\exp(-z\ell)] & ;\ \ell > 0 \end{array}\right\}. \tag{2.80}$$

The limiting behavior of the infinite product expansions $\Pi(\pm\omega,\beta)$ in (2.39) is deduced from an infinite product expansion of the gamma function (Whitehead, 1951). To check whether $T(\omega)$ has the correct asymptotic behavior, $Z^{-\nu}$, is substituted for $T(z)$ in (2.79). The result is given by

$$\lim_{\substack{|\omega|\to\infty \\ -\pi<\arg(\omega)<\pi}} \left[T(\omega)\right] = \begin{cases} \frac{1}{\pi}\left[\frac{\kappa-1}{\kappa+1}\right]\left(\int_0^\infty \frac{z^{-\nu}}{\omega+z}\, dz + \int_0^\infty \frac{z^{-\nu}\cos(2zb)}{\omega+z}\, dz \right) + O\left[\frac{1}{\omega}\right], & \ell = 0 \\ O\left[\frac{1}{\omega}\right], & \ell > 0 \end{cases} \tag{2.81}$$

For $0 < \mathrm{Re}(\nu) < 1$, these integrals can be evaluated by comparison with the appropriate Stieltjes' transforms (Bateman, 1954), and the results are given by

$$\int_0^\infty \frac{z^{-\nu}}{\omega+z}\, dz = \frac{\pi\, \omega^{-\nu}}{\sin(\nu\pi)} \tag{2.82}$$

and

$$\lim_{\substack{|\omega|\to\infty \\ -\pi<\arg(\omega)<\pi}} \left\{ \int_0^\infty \frac{z^{-\nu}\cos(2zb)}{\omega+z}\, dz \right\} = O\left[\frac{1}{\omega}\right] . \tag{2.83}$$

Substituting these results into (2.81), together with the assumed asymptotic expression for $T(\omega)$, yields

$$\omega^{-\nu} \to \left\{ \begin{array}{ll} \left[\frac{\kappa-1}{\kappa+1}\right] \frac{\omega^{-\nu}}{\sin(\nu\pi)} + O\left[\frac{1}{\omega}\right] & , \ \ell = 0 \\ O\left[\frac{1}{\omega}\right] & , \ \ell > 0 \end{array} \right\} . \qquad (2.84)$$

Comparing coefficients of $\omega^{-\nu}$ in (2.84) gives the correct result (2.39), which is repeated here for clarity.

$$\nu = \left\{ \begin{array}{ll} 1 - \max\left(0 \, , \frac{1}{\pi} \arcsin\left[\frac{\kappa-1}{\kappa+1}\right]\right) & ; \ \ell = 0 \\ 1 & ; \ \ell > 0 \end{array} \right\} . \qquad (2.39)$$

Thus, the correct edge condition is satisfied by the solution given in Section 2.3.

2.5 Surface Waves in the Dielectric Slab

The existence of surface modes in the dielectric slab was previously mentioned as being attributed to the poles of $R^{-1}(\alpha)$. In order to show the behavior of $R(\alpha)$, we factor it into an equivalent form

$$R(\alpha) = \frac{1}{\kappa\xi\tau} [(CO)\cdot(CE)] \ , \qquad (2.85)$$

where

$$(CE) = \tau \sinh(\tau t) + \kappa\xi \cosh(\tau t) \qquad (2.86)$$

and

$$(CO) = \tau \cosh(\tau t) + \kappa\xi \sinh(\tau t) \ . \qquad (2.87)$$

Equations (2.86) and (2.87) are respectively the determinantal or characteristic equations for the longitudinal propagation constants α for even and odd TM-type surface modes within the dielectric slab (Collin, 1960).

We now write equation (2.1), which gives the magnetic intensity inside the slab, in terms of the even and odd characteristic equations

$$(H_y)_A = \frac{1}{2}\int_{\sigma}\left(\frac{\kappa\, F(\xi|_{\sigma_1})\exp(-j\alpha b)}{\pi\exp(\xi\ell)}\right)\left(\frac{\cosh[\tau(z-\ell-t)]}{(CE)}+\frac{\sinh[\tau(z-\ell-t)]}{(CO)}\right)\exp(-j\alpha x)d\alpha\ . \qquad (2.88)$$

The integrand in (2.88) has simple poles at those values of α where (2.86) and (2.87) are zero and branch points at $\alpha = \pm k_o$. The corresponding branch cuts of $\xi(\alpha)$ are shown in Figure 7. The magnetic intensity of the surface modes can be evaluated by closing the contour of integration in (2.88) in the lower half α-plane for $x > 0$ and in the upper half α-plane for $x < 0$. Such closed contours are shown in Figure 7. It can be seen that in both cases; i.e., $x > 0$ and $x < 0$, the appropriate contour encloses all of the poles of the function $R^{-1}(\alpha)$. An application of the Cauchy theorem to the closed contour integrations yields the following results: (1) The radiation field can be identified with the contour integration along the branch singularity of $\xi(\alpha)$. (2) The surface modes are identified with the residues of the integrand of (2.88) evaluated at the singularities of $R^{-1}(\alpha)$.

Before writing explicit expressions for the surface modes, some nomenclature for identifying each mode is presented. When $\kappa > 1$ and real,

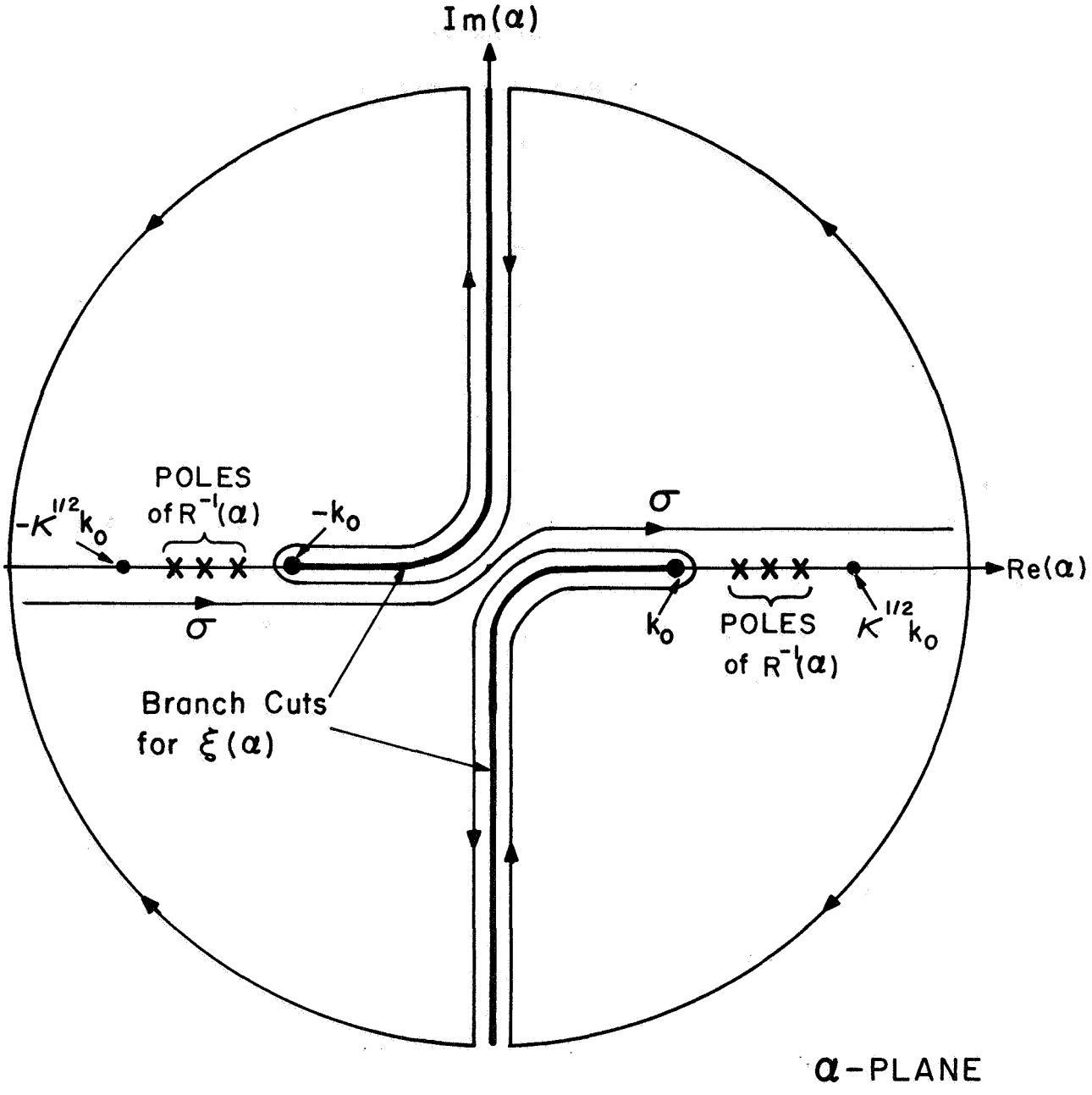

Figure 7. The paths of integration for determining the fields in the dielectric slab.

equations (2.86) and (2.87) have a number of real zeros which lie in the interval $(k_o, \kappa^{1/2} k_o)$. We assign to the zeros of the even characteristic equation (2.86) even integers, so that if there are M+1 such zeros, we obtain $(\alpha_0 < \alpha_2 < \ldots < \alpha_M)$. For the odd equation (2.87), the zeros are given by $(\alpha_1 < \alpha_3 < \ldots < \alpha_N)$. Moreover, the zeros of the even and odd characteristic equations are interleaved (Collin 1960), and α_0 is always the smallest of the set of values. We identify each surface mode with the corresponding value of α_j, i.e., the j-th mode is of the TM_{jo}-type with respect to the x-direction. If j is even or odd, we mean respectively, even or odd surface waves. Finally, the TM_0 surface mode has no cut-off frequency, so that when $\kappa > 1$, we always have at least one surface mode launched within the slab.

We are now in a position to write the expressions for the magnetic intensity of the surface modes. When (m = 0,1,..., M) we express the even modes as

$$H_y^m = \left[\frac{j \kappa F(\xi) \cosh[\tau(z-\ell-t)] \exp[-j\alpha(|x|-b)]}{\exp(\xi\ell) \frac{\partial}{\partial\alpha}(CE)} \right]_{\alpha = \alpha_m} . \qquad (2.89)$$

For (n = 1,3,...,N) the odd modes are given by

$$H_y^n = \left[\frac{j \kappa F(\xi) \sinh[\tau(z-\ell-t)] \exp[-j\alpha(|x|-b)]}{\exp(\xi\ell) \frac{\partial}{\partial\alpha}(CO)} \right]_{\alpha = \alpha_n} . \qquad (2.90)$$

We see that both types of modes represent waves which travel away from the waveguide aperture in the x-direction and without attenuation. Furthermore, as the dielectric slab is moved away from the waveguide aperture, the launching of surface waves becomes increasingly difficult.

This difficulty is due to the factor $\exp(\xi \ell)$ in the denominator of (2.89) and (2.90), and represents an exponential damping of the surface mode excitation with increasing ℓ.

2.6 Radiation Field in the Open-Region

The radiation fields in the open-regions C and E of Figure 2 may be evaluated from the integrations indicated by the corresponding Fourier transforms, viz., equations (2.3) and (2.5). However, the saddle-point method of integration (Collin, 1960) may be employed instead, and the radiation fields are obtained directly from the spectral weight coefficients $C(\gamma)$ and $E(\alpha)$. These weight coefficients need only be known in the visible range, i.e., $0 \leq \left(\alpha \ , \ \gamma\right) \leq k_o$. This limited knowledge is desirable from the standpoint of numerical computation.

Before presenting the results of the saddle-point method of integration, we digress for the moment to investigate the effect that a dielectric or plasma slab has on a uniform plane wave. The result of this investigation will prove most useful in interpreting the equations for the radiated fields.

2.6.1 Effect of the Slab on Plane Waves

Before considering the expressions for the radiation fields, we first determine the influence that a dielectric of plasma slab has on a uniform plane wave. Figure 8 shows the incident field denoted by (E_i, H_i). The direction of propagation with respect to the normal of the slab is given by θ. The reflected and transmitted waves are (E_r, H_r) and (E_t, H_t) respectively, and the associated coefficients of reflection and transmission are given by $\overline{R}$ and $\overline{T}$ respectively. Also shown in Figure 8 are the forward and backward traveling waves (E_f, H_f) and $E_b, H_b)$ inside the slab, and the angle of refraction ψ.

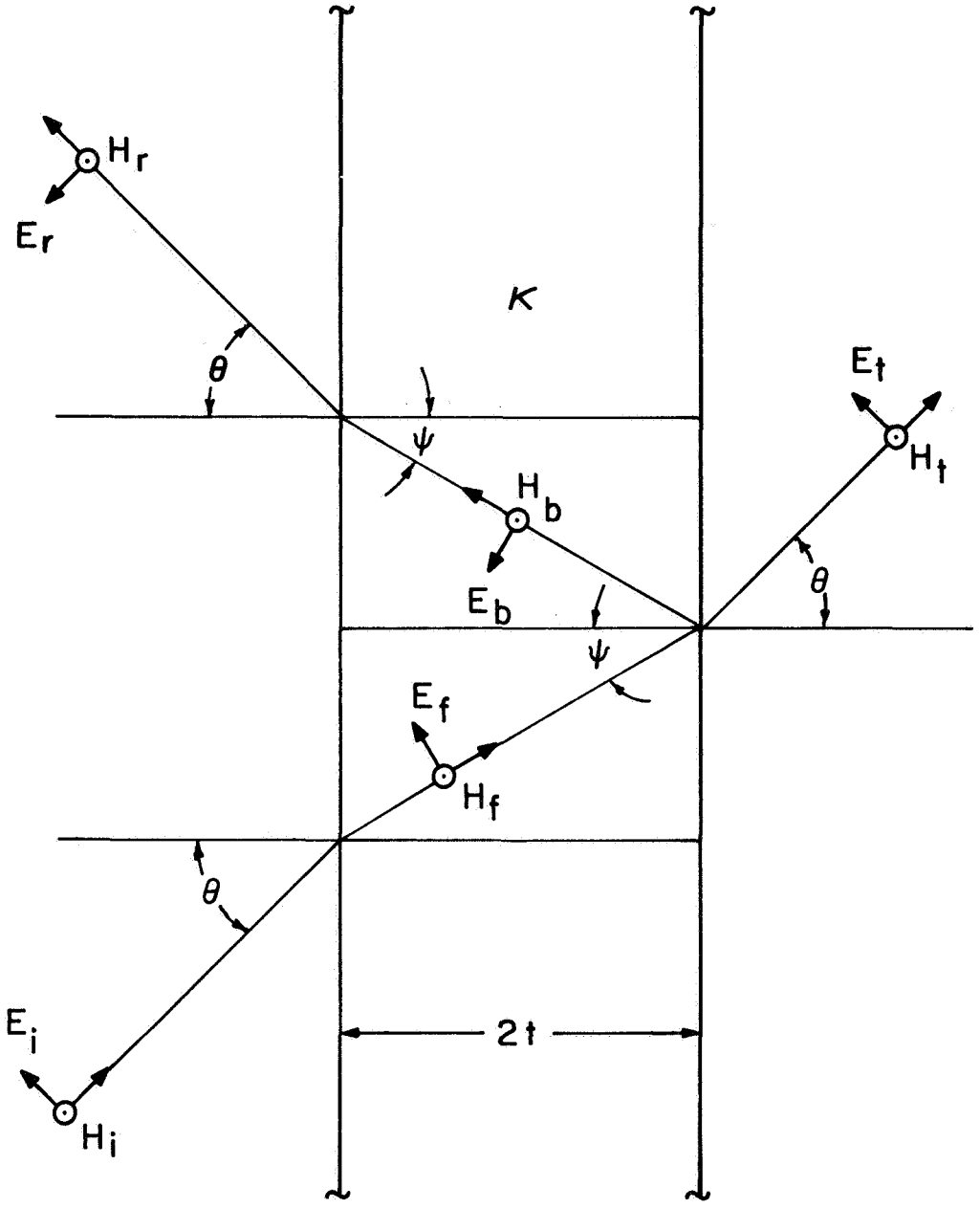

Figure 8. Uniform plane wave incident onto a dielectric or plasma slab having a thickness 2t and a relative dielectric constant κ.

A lengthy but straightforward solution for the coefficients of reflection and transmission yields

$$\overline{R}(\alpha) = \frac{Q(\alpha)}{R(\alpha)} \tag{2.91}$$

and

$$\overline{T}(\alpha) = [R(\alpha)]^{-1} \quad , \tag{2.92}$$

where $\alpha = k_o \sin(\theta)$. The functions, $R(\alpha)$ and $Q(\alpha)$, are identical to those employed in the preceding analysis and are given by (2.23) and (2.24) respectively. An inspection of the function $Q(\alpha)$ indicates that there are several angles of indidence θ for which there is no reflection from the slab. Expanding (2.24) in terms of its zeros yields

$$Q[k_o \sin(\theta)] = \frac{(\kappa-1)\ (\kappa+1)\ \sin\left[2t\ k_o\sqrt{\kappa-\sin^2(\theta)}\right]}{2j\ \kappa^{3/2}\ \cos(\theta)\ \cos(\psi)}$$

$$\left[\sin(\theta) + \sqrt{\frac{\kappa}{\kappa+1}}\right]\left[\sin(\theta) - \sqrt{\frac{\kappa}{\kappa+1}}\right] . \tag{2.93}$$

The angles for zero reflection occur when $\kappa = 1$ (slab removed), at the Brewster angles θ_B (Jordan, 1950)

$$\theta_B = \pm \arcsin \sqrt{\frac{\kappa}{\kappa+1}} \quad , \tag{2.94}$$

and at certain other angles determined from the relation

$$\sin\left[2t\ k_o\sqrt{\kappa-\sin^2(\theta)}\right] = 0 . \tag{2.95}$$

The critical angles given by (2.95) are dependent not only on the relative dielectric constant of the slab, but also depend on the thickness. An investigation of these angles shows that they correspond to a matched condition of the directional wave impedances as observed on each side of the left-hand air-slab interface (cf. Figure 8). A simple example occurs when the angle of incident θ is zero, and the slab thickness $2t$ is equal to an integral number of half-wavelength as determined inside the slab.

When the slab is a plasma, i.e., $\kappa < 1$, we find no angles θ where zero reflection occurs. Rather, the coefficient of reflection approaches unity as $\kappa \to -\infty$, indicating transmission through the slab is cut-off for all angles of incidence. An asymptotic expression for the reflection coefficient is given by

$$\lim_{\kappa \to -\infty} |\bar{R}| = \frac{|\kappa^{1/2}| \cos(\theta)}{|[2j + |\kappa^{1/2}| \cos(\theta)]|} \to 1 \qquad (2.96a)$$

On the other hand, the transmission factor $\bar{T}$ introduces a severe attenuation of the transmitted wave when the slab thickness is large or the relative dielectric constant is made negative. An asymptotic expansion for the coefficient of transmission is given by

$$\lim_{\kappa \to -\infty} |\bar{T}| = \frac{2 \exp(-2t\, k_o |\kappa^{1/2}|)}{|[2j + |\kappa^{1/2}| \cos(\theta)]|} \to$$

$$O[\exp(-t\, |\kappa^{1/2}|)] \qquad (2.96b)$$

We now have expressions for the coefficients of reflection and transmission for a uniform plane wave incident onto the slab. This information will be employed for a geometric interpretation of the solution of the problem at hand in the next section.

2.6.2 Pattern in the Forward Direction

The radiation field in region E of Figure 2 is obtained by applying a transformation of variable to the Fourier transform expression for the magnetic intensity. This transformation is given by

$$\left\{ \begin{array}{ll} \xi = j\, k_o \cos(\phi) & x = r \sin(\theta) \\ \alpha = k_o \sin(\phi) & (z - \ell - 2t) = r \cos(\theta) \end{array} \right\} . \qquad (2.97)$$

Employing (2.97) in (2.5) yields

$$(H_y)_E = \int_{c'} E\left[k_o \sin(\phi)\right] \exp[-j\, k_o r \cos(\theta-\phi)]\, k_o \cos(\phi)\, d\phi. \qquad (2.98)$$

Applying the method of saddle-point integration to (2.98) yields an asymptotic expression for the radiated field

$$\lim_{r\to\infty} (H_y)_E = \sqrt{\frac{k_o \pi}{2\, r}}\, \cos(\theta)\, E\left[k_o \sin(\theta)\right] \exp[-j(k_o r - \pi/4)] \quad . \qquad (2.99)$$

The radiation pattern in the forward direction is obtained by substituting the solution for E given by (2.44) into (2.99)

$$\text{PATTERN}(\theta) = \left| F\left[jk_o \cos(\theta)\right] \; \overline{T}\left[k_o \sin(\theta)\right] \right| , \qquad (2.100)$$

where F is the function constructed by the modified function-theoretic technique, viz., equation (2.35), and $\overline{T}$ is the transmission coefficient of the slab given by (2.92). The total power radiated in the forward direction is obtained from the expression

$$P_{rad} = \frac{1}{(1+\delta_p^o)\, b\, \pi\, k_o} \int_0^{\pi/2} \left| \frac{F[jk_o \cos(\theta)]}{R[k_o \sin(\theta)]} \right|^2 d\theta , \qquad (2.101)$$

where integration is only over positive angles of θ due to the symmetry of the fields. The observation angle θ and polar coordinates (r,θ) for region E are shown in Figure 9.

An examination of the pattern function (2.100) reveals that there are nulls in the forward pattern for those directions where $F\left[jk_o \cos(\theta)\right] = 0$. The angles θ corresponding to these nulls can be identified with the directions of propagation in composite plane-wave representation of the waveguide modes (cf. Figure 10a). However, there is a maximum in the pattern at the angle corresponding to the incident mode exciting the guide. The salient features of the forward pattern can be summarized as follows:

$$\text{PATTERN NULLS:} \quad \left[\theta = \pm \arcsin\left(\frac{s\pi}{b}\right) \; ; \; s \neq p \; , \; s \leq N\right] \qquad (2.102)$$

$$\text{PATTERN MAX:} \quad \left[\theta = \pm \arcsin\left(\frac{p\pi}{b}\right) \right] , \qquad (2.103)$$

where only propagating modes are considered, i.e., $N \leq b\, k_o/\pi$.

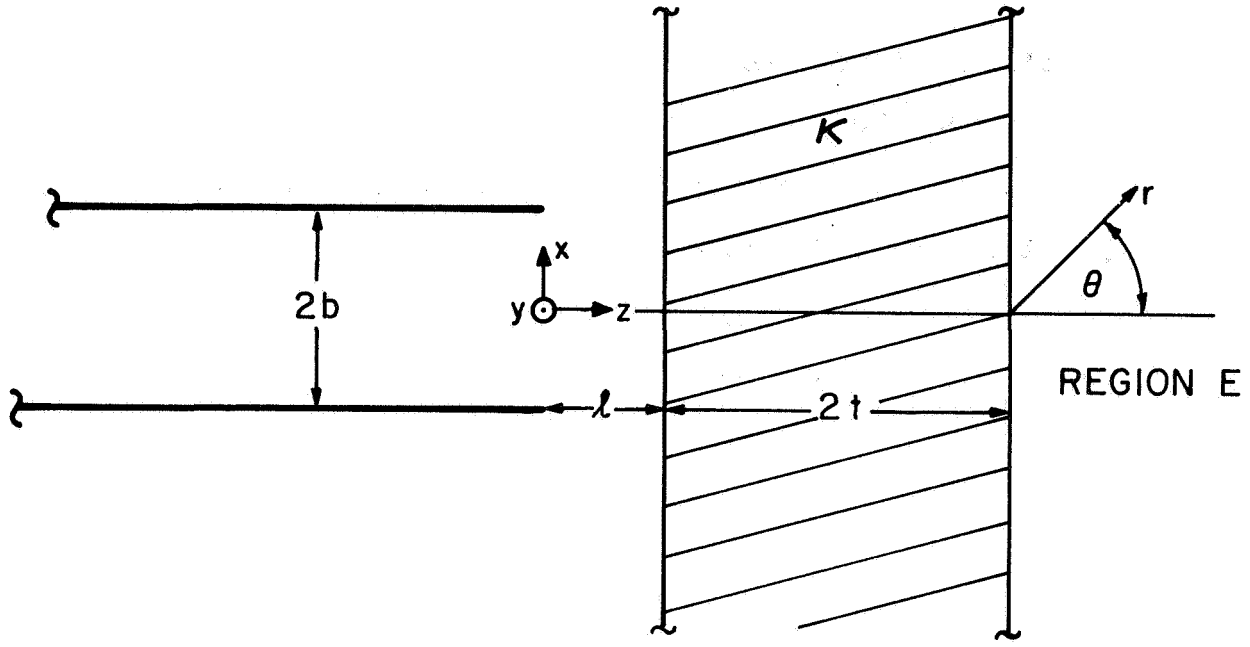

Figure 9. The observation angle θ in the forward direction.

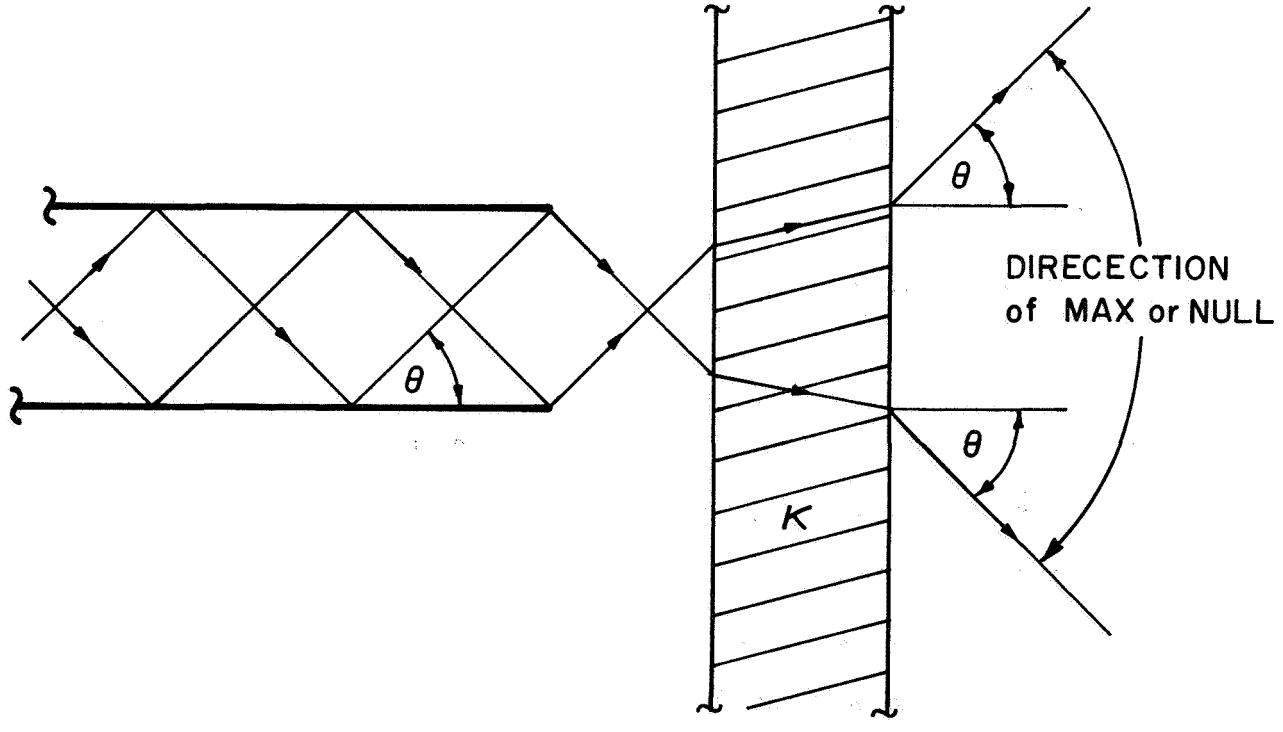

Figure 10. The direction of max or null in the forward region.

2.6.3 Pattern in the Backward Direction

The radiation pattern in the backward direction, region C, is obtained in exactly the same manner as was presented in Section 2.6.2 for the forward region. The results are given by

$$\lim_{r\to\infty} (H_y)_C = \sqrt{\frac{k_o \pi}{2\, r}}\ \cos(\theta)\ C[k_o \sin(\theta)] \cdot$$

$$\exp[-j(k_o r - k_o b + \pi/4)] \qquad (2.104)$$

$$\text{PATTERN}(\theta) = \Big| F\left[-jk_o \cos(\theta)\right] +$$

$$\overline{R}\left[k_o \sin(\theta)\right]\ F\left[jk_o \cos(\theta)\right] \exp\left[-2j\, k_o \ell \cos(\theta)\right] \Big| \qquad (2.105)$$

and

$$P_{rad} = \frac{1}{(1+\delta_p^o)\, b\, \pi\, k_o} \int_0^{\pi/2} \Big| F\left[-jk_o \cos(\theta)\right] +$$

$$\frac{Q'[k_o \sin(\theta)]}{R'[k_o \sin(\theta)]}\ F\left[jk_o \cos(\theta)\right] \Big|^2 d\theta \ . \qquad (2.106)$$

The angle of observation θ for the backward direction is shown in Figure 11. The pattern function, as given by (2.105), has a geometrical interpretation. We note that the radiation field is composed of two parts. The first is that due to $F[-jk_o \cos(\theta)]$, which we identify with the direct field radiated from the guide aperture. The second part is due to $F[jk_o \cos(\theta)]$, which is the field radiated into the forward

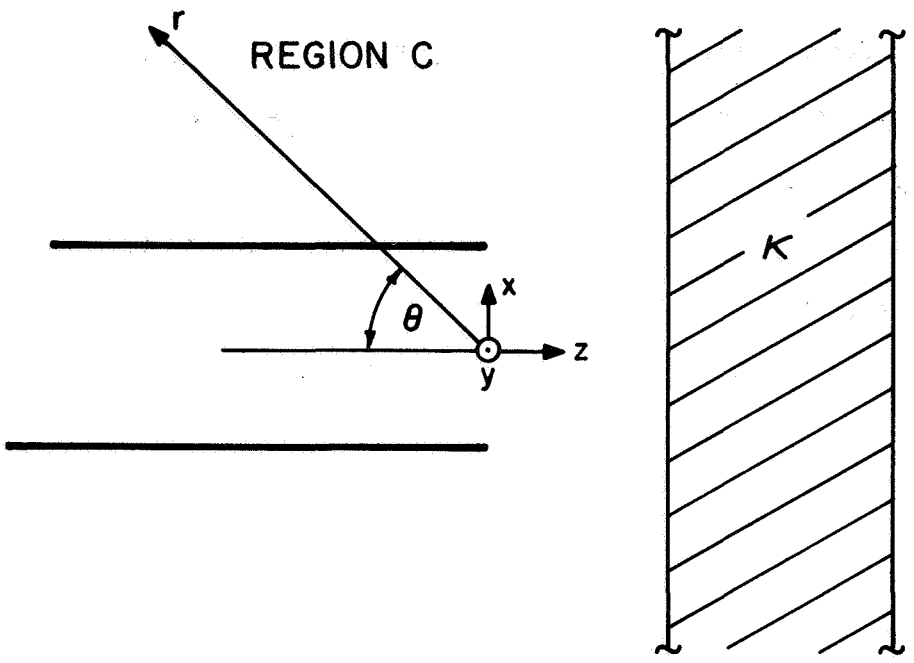

Figure 11. The observation angle θ in the backward direction.

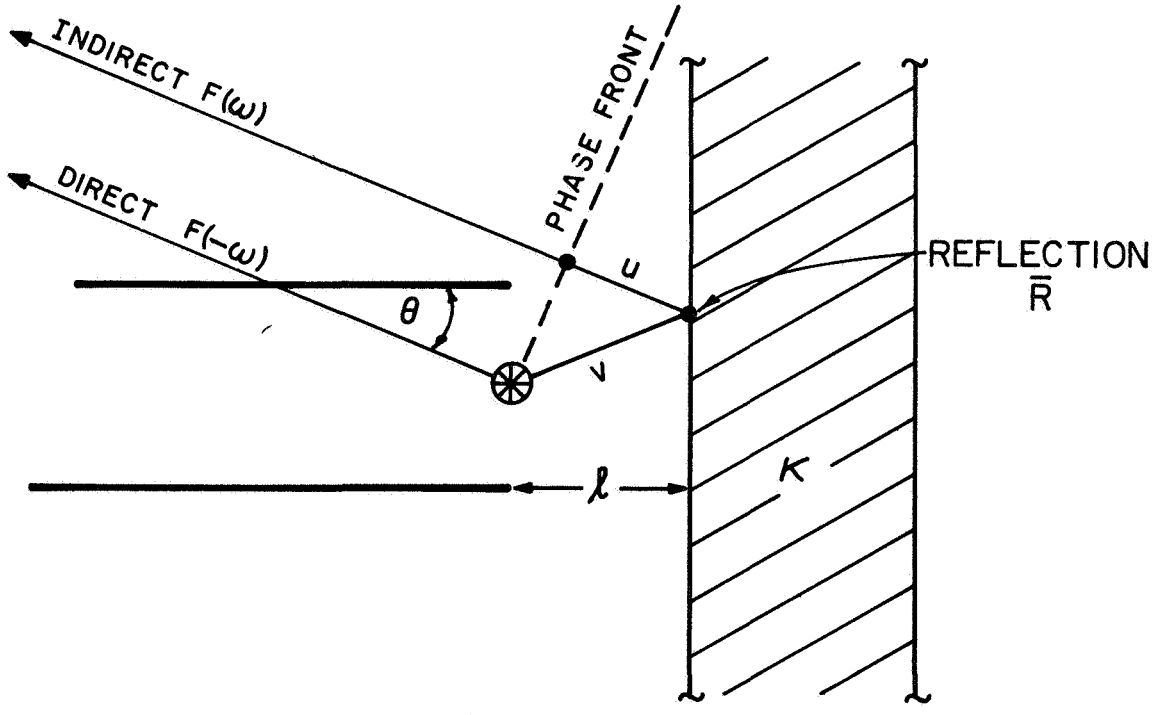

Figure 12. The composite field in the backward direction showing the path difference between the direct and indirect fields. $u + v = 2\ell \cos(\theta)$.

direction. This forward field is modified by the function $\overline{R}$, the reflection coefficient from the slab, and a phase difference $\exp[-2jk_o \ell \cos(\theta)]$, which is the path difference between the direct and reflected fields. Figure 12 shows both fields being emitted from a common point, viz., the center of the waveguide aperture, and the path difference between the direct and indirect fields, i.e., $u + v = 2\ell \cos(\theta)$ (cf. Figure 12).

3. SOLUTIONS FOR RELATED PROBLEMS

In order to show the versatility of the modified function-theoretic technique, we present the solutions for two other open-region problems. These problems again represent a modification to the canonical problem, and their geometry is constructed by introducing a longitudinal inhomogeneity in one of the open-regions.

The first of the modified problems is shown in Figure 13, and represents an open-ended waveguide radiating into a reflecting plane. Such a geometry is closely related to large aperture reflector antennas. The solution for this problem is constructed from the function

$$H(\omega) = F_1(\omega)\ S(\omega)\ , \tag{3.1}$$

where $F_1(\omega)$ is again the canonical function given by (2.36). The portion of $H(\omega)$ which represents the departure from the canonical function is represented by $S(\omega)$. We require $S(\omega)$ to have a simple pole at $\omega = \beta_p$ and a branch cut along the path σ_3 (cf. Figure 4). These requirements are identical to those for $T(\omega)$, the modifying function for the problem in section 2. In fact, whenever there is a longitudinal inhomogeneity facing or opposite the waveguide aperture, the modifying function will have these requirements.

A solution for the mode and weight coefficients in regions B and C are given by

$$B_m = - \frac{(-1)^m\ H(-B_m|_{\sigma_3})}{b\ \beta_s\ (1+\delta_s^o)} \tag{3.2}$$

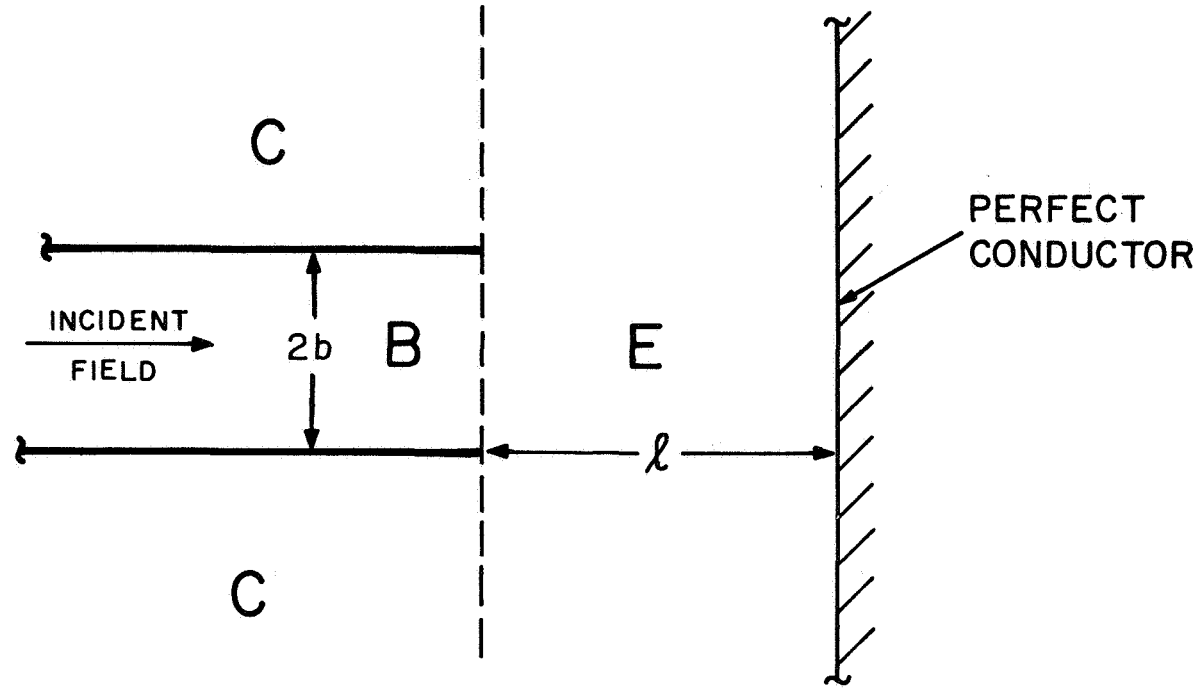

Figure 13. Waveguide radiating into a reflecting wall.

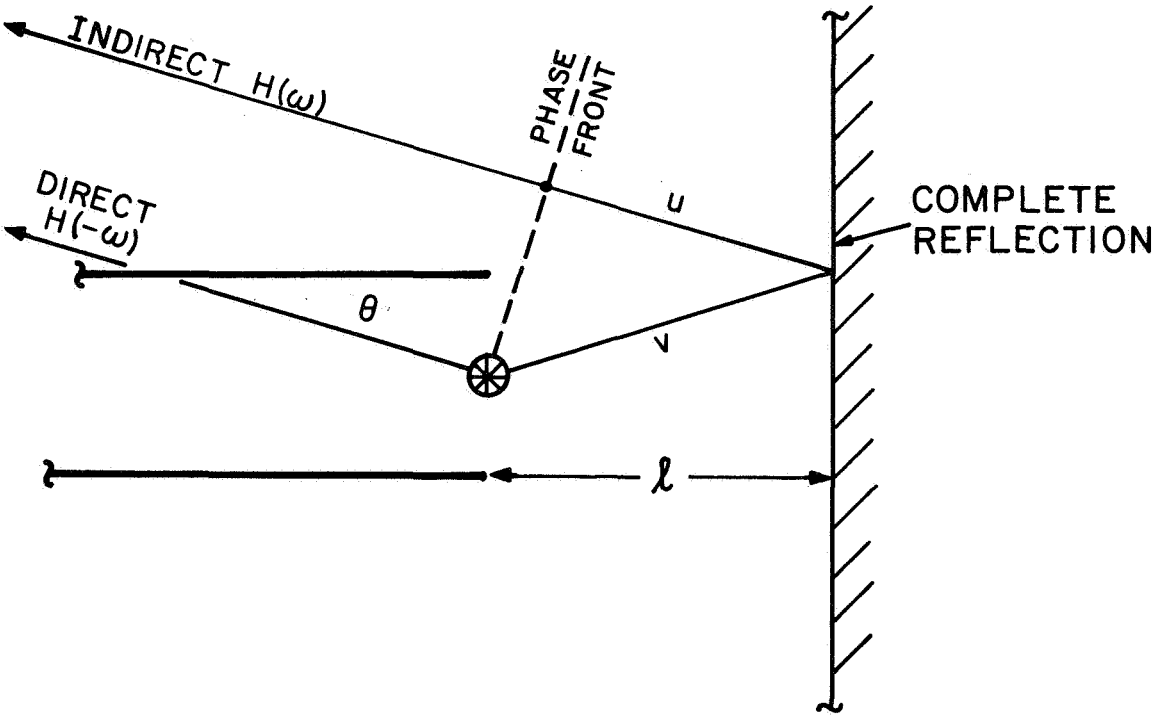

Figure 14. The composite field for a waveguide radiating into a reflecting wall. $u + v = 2\ell \cos(\theta)$.

and

$$C(\gamma) = \frac{1}{\pi\ \eta}\ [H(-\eta|_{\sigma_3}) + H(\eta|_{\sigma_1})e^{-2\eta\ell}] \quad . \tag{3.3a}$$

The normalization condition is obtained from the relationship

$$H(\beta_p|_{\sigma_1}) = b\ \beta_p\ (-1)^p\ (1+\delta_p^o). \tag{3.3b}$$

The radiation pattern is given by

$$\text{PATTERN}(\theta) = \left| H\left[-jk_o\cos(\theta)\right] + H\left[jk_o\cos(\theta)\right]\ e^{-2j\ k_o\ \ell\cos(\theta)} \right| . \tag{3.4}$$

The resulting expressions for the branch discontinuity and the auxiliary integral equation are, respectively,

$$S(-\omega|_{\sigma_3}) - S(-\omega|_{\sigma_4}) = 2\pi j\ \mu(\omega)\ S(\omega|_{\sigma_1}) \tag{3.5}$$

and

$$S(\omega) = \frac{1}{\omega-\beta_p} + \int_{\sigma_1} \frac{\mu(z)\ S(z)}{\omega+z}\ dz \quad . \tag{3.6}$$

The partial kernel $\mu(\xi)$ for this problem is given by

$$\mu(\xi) = -\frac{e^{-2\xi\ell}\ \sin(\alpha b)\ \exp(-j\alpha b)}{\pi}\ \frac{F_1(\xi|_{\sigma_1})}{F_1(-\xi|_{\sigma_3})} \quad . \tag{3.7}$$

As for the problem in section 2, we see that the radiated field in region c is composed of two fields (cf. Figure 14). Referring to equation (3.4), we see that the direct field is given by $H(-\omega)$. The indirect field is obtained by reflecting $H(\omega)$ from the reflecting wall with its phase retarded by the path length $\mu + \nu = 2\ \ell\cos(\theta)$.

The geometry of the second problem we wish to discuss is shown in Figure 15. This problem represents radiation from a flanged waveguide. Since the longitudinal inhomogeneity is placed in back of the waveguide aperture-plane, we would not expect the modifying function to have a

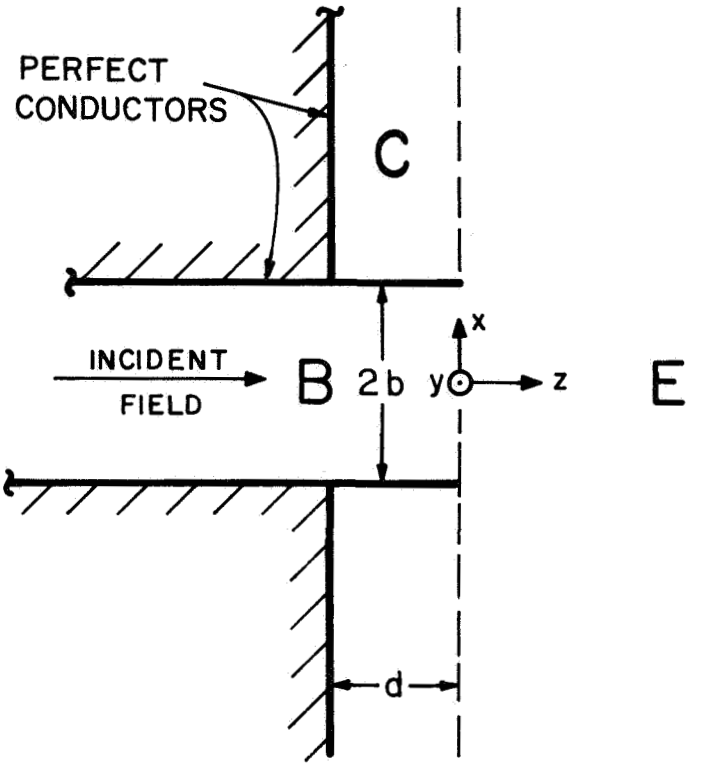

Figure 15. Flanged parallel-plate waveguide.

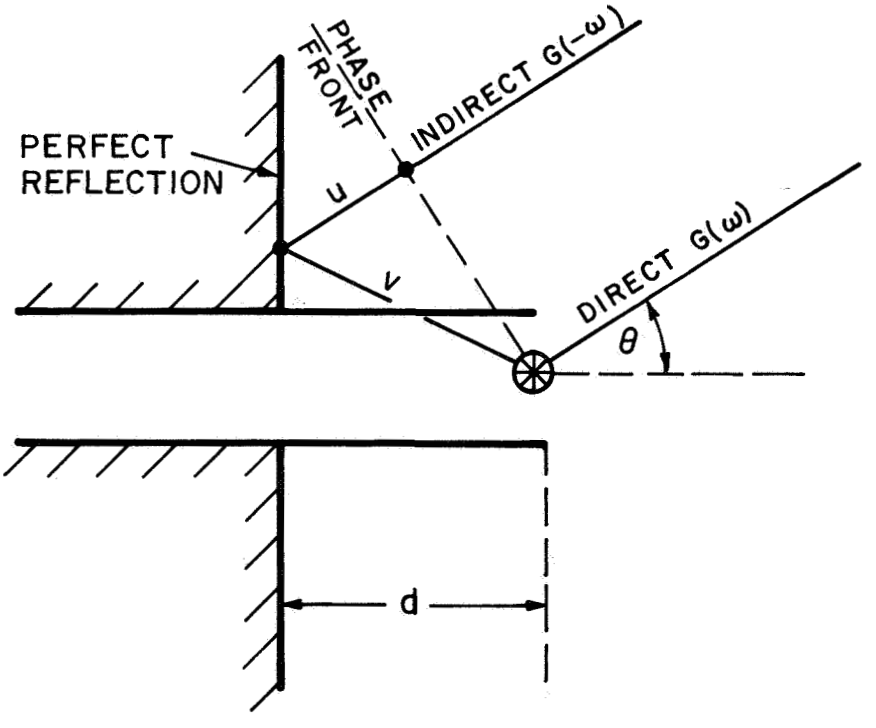

Figure 16. The composite field for the flanged waveguide. $u + v = 2\ell \cos(\theta)$.

branch singularity along the path σ_3 (cf. Figure 4), and this is indeed the case.

We again write the constructed function in the following form:

$$G(\omega) = F_1(\omega)\ U(\omega) \quad . \tag{3.8}$$

We find that an analysis of the problem requires the modifying function $U(\omega)$ again have a simple pole at $\omega = \beta_p$; however, for this geometry, the branch singularity is along the path σ_1 instead of σ_3. The solution for this problem is given as follows:

$$B_s = \frac{-(-1)^s\ G(-\beta_s|_{\sigma_3})}{b\ \beta_s\ (1+\delta_s^o)} \tag{3.9}$$

and

$$E(\xi) = \frac{e^{-j\alpha b}}{\pi\ \xi}\left[\ G(\xi|_{\sigma_1}) + G(-\xi|_{\sigma_3})e^{-2\xi d}\right] \tag{3.10a}$$

The normalization condition is determined from the relationship

$$G(\beta_p|_{\sigma_1}) = b\ \beta_p\ (-1)^p\ (1+\delta_p^o) \quad . \tag{3.10b}$$

The radiation pattern is given by

$$\text{PATTERN}(\theta) = \Big|\ G\left[jk_o\cos(\theta)\right] + G\left[-jk_o\cos(\theta)\right]\ \exp\left[-2jk_o d\cos(\theta)\right]\ \Big| \quad . \tag{3.11}$$

As in the previous examples, the radiation field can be interpreted in terms of the direct and indirect fields which originate from a common point (cf. Figure 16). The expressions for the branch discontinuity and the auxiliary integral equation are as follows:

$$U(\omega|_{\sigma_1}) - U(\omega|_{\sigma_2}) = 2\pi j\ \lambda(-\omega)\ U(-\omega|_{\sigma_3}) \tag{3.12}$$

and

$$U(\omega) = \frac{1}{\omega-\beta_p} + \int_{\sigma_3} \frac{\lambda(z)\ U(z)}{z+\omega}\ dz \quad . \tag{3.13}$$

The partial kernel $\lambda(\xi)$ is given by

$$\lambda(-\xi) = \frac{e^{j\alpha b}\ \sin(\alpha b)\ \exp(-2\xi d)}{\pi} \frac{F_1(-\xi|_{\sigma_3})}{F_1(\xi|_{\sigma_1})} \tag{3.14}$$

Another interesting problem is that of a flanged waveguide combined with a dielectric or plasma slab covering the guide aperture. Such is the case for radiation from an antenna flush mounted on the surface of a rocket with a plasma sheath covering the aperture-plane. The solution for this problem can be obtained by the modified function-theoretic technique. However, since the canonical problem is modified on both sides of the aperture-plane, we obtain two auxiliary equations. The form of the constructed function is given by

$$J(\omega) = F_1(\omega)\ [L(\omega) + M(\omega)] \quad . \tag{3.15}$$

The modifying functions, $L(\omega)$ and $M(\omega)$, have branch singularities along σ_1 and σ_3 respectively (cf. Figure 4). The simultaneous solution of the two auxiliary integral equations is not a simple one, since there is a coupling between $L(\omega)$ and $M(\omega)$ in the two equations. Due to the complexity of this problem, we give no results, but only indicate that a solution is possible.

A final note relating to the modified problems just discussed is that in each case the correct edge condition may be shown to be satisfied. This is accomplished by comparing the asymptotic form of the auxiliary integral equation with the appropriate Stieltjes transform (cf. Section 2.4.2).

4. EXTENSION TO CIRCULAR GEOMETRY

The results that have been given thus far are concerned with the excitation of inhomogeneously filled open-regions by parallel-plate waveguides. Such problems are physically not realizable, but their solutions give a tremendous insight into the form of the solution for physically obtainable problems. Each of the problems discussed in the previous sections can be solved by the modified function-theoretic technique when the geometry is circular, and the electromagnetic fields have rotational symmetry. The only difficulty is that the factor $N(\omega)$ employed in the construction of the canonical function $F_1(\omega)$, no longer has a closed form expression. We may, however, employ an integral formulation for $N(\omega)$ given by Mittra and Bates (1965)

$$N(\omega) = \exp\left[\frac{b\omega}{\pi}\left(1 - C_e + \ln\left(\frac{2\pi}{k_o b}\right)\right) + j\frac{b\omega}{2}\right] N_1(\omega) \quad , \qquad (4.1)$$

where

$$N_1(\omega) = \lim_{\substack{a,c\to\infty \\ a-c=b}} \left[\frac{\Pi(\omega,\eta)}{\Pi(\omega,\xi)}\right] =$$

$$\exp\left\{\frac{b}{\pi}\int_0^\infty \left[\ln\left(1 - \frac{\omega}{\sqrt{z^2-k_o^2}}\right) + \frac{\omega}{\sqrt{z^2-k_o^2}}\right]\left[\frac{2}{\pi z b}\left[N_o^2(zb) + J_o^2(zb)\right]^{-1}\right] dz\right\} . \qquad (4.3)$$

In Figure 17, we show the radii of the small and large waveguides, viz., b and a, for the associated closed-region problem. as the outer guide radius becomes infinitely large, (4.3) is determined as the limit of the quotient of the infinite product expansions for regions C and E. The functions J_o and N_o employed in (4.3) are respectively zero order Bessel functions the first and second kind. The function $N_1(\omega)$ is seen

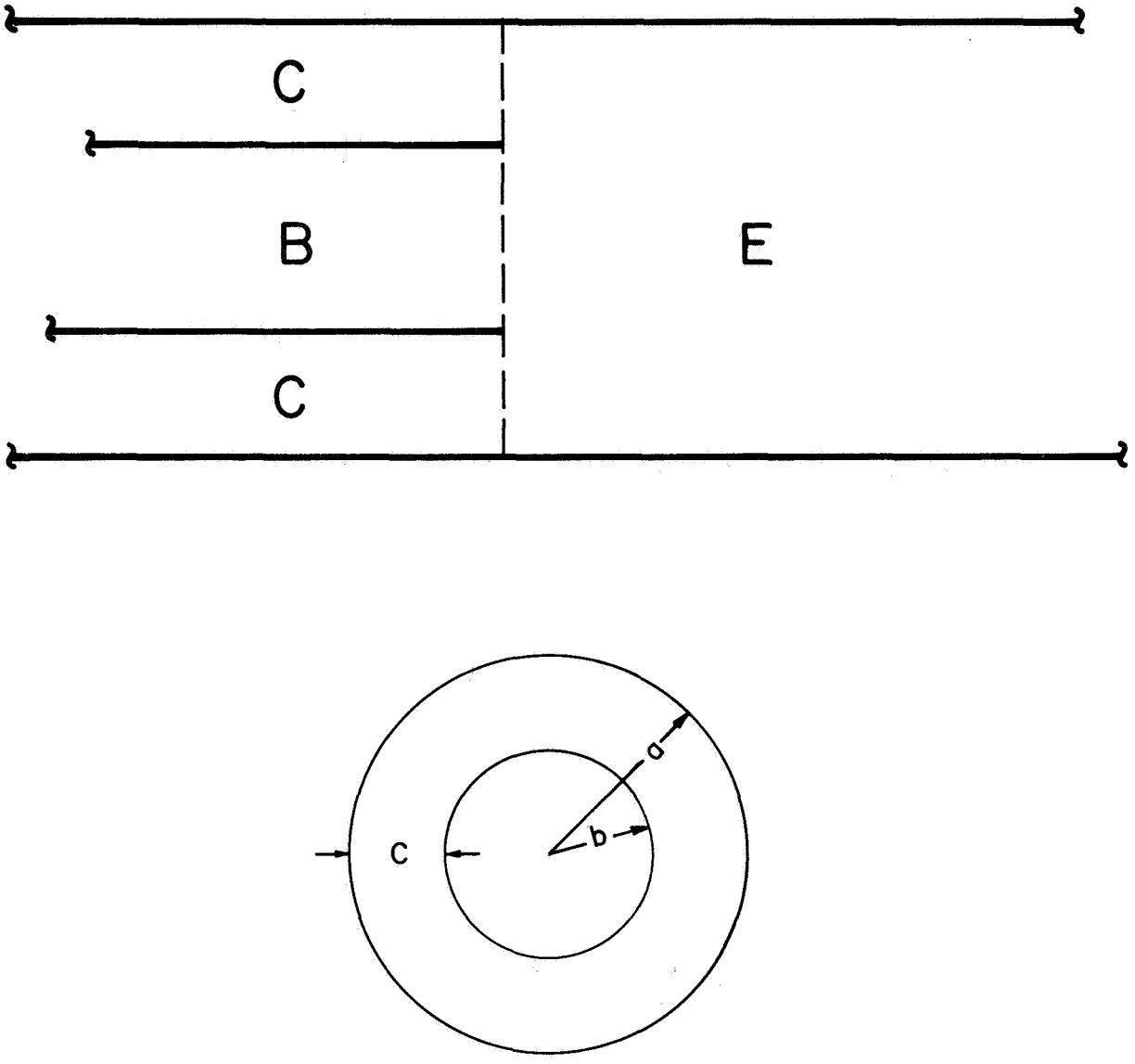

Figure 17. The canonical closed-region problem in circular geometry.

to have a branch point at $\omega = jk_o$. The branch cut for $N_1(\omega)$ is chosen along the path σ_1 (cf. Figure 18).

Although (4.3) can not be written in a closed-form, we may approximate it by a numerically truncated integral. We note that for large values of z the integrand of (4.3) is nearly equal to the corresponding intergrand in the parallel-plate case, which does have a closed-form expression. That is to say, $[2/(\pi bz)][N_o^2(zb) + J_o^2(zb)]^{-1} \to 1$ for even moderately large values of z, e.g., this function equals 0.95 when zb = 1. We, therefore, write (4.3) in the following approximate form:

$$N_1(\omega) \cong \bar{N}_1(\omega) \exp\left\{ \frac{-b}{2\pi} \int_0^L \left[\ln\left(1 - \frac{\omega}{\sqrt{z^2-k_o^2}}\right) + \frac{\omega}{\sqrt{z^2-k_o^2}} \right] \left[\left[\frac{2}{\pi\, b\, z}\right] \left[J_o^2(zb) + N_o^2(zb)\right]^{-1} - 1 \right] dz \right\} . \tag{4.4}$$

The function $\bar{N}_1(\omega)$ is the parallel-plate canonical function given by (2.38). The truncation point L is determined from a given numerical accuracy criterion.

Aside from the integral expression (4.3) for $N_1(\omega)$, we are able to obtain two other useful relationships which aid in the numerical computation of this function. The method employed in obtaining these relationships is to find the limiting behavior of the product $[n_1(\omega)n_1(-\omega)]$ as the outer waveguide radius becomes infinite. Here we have written n_1 as the closed-region form of N_1

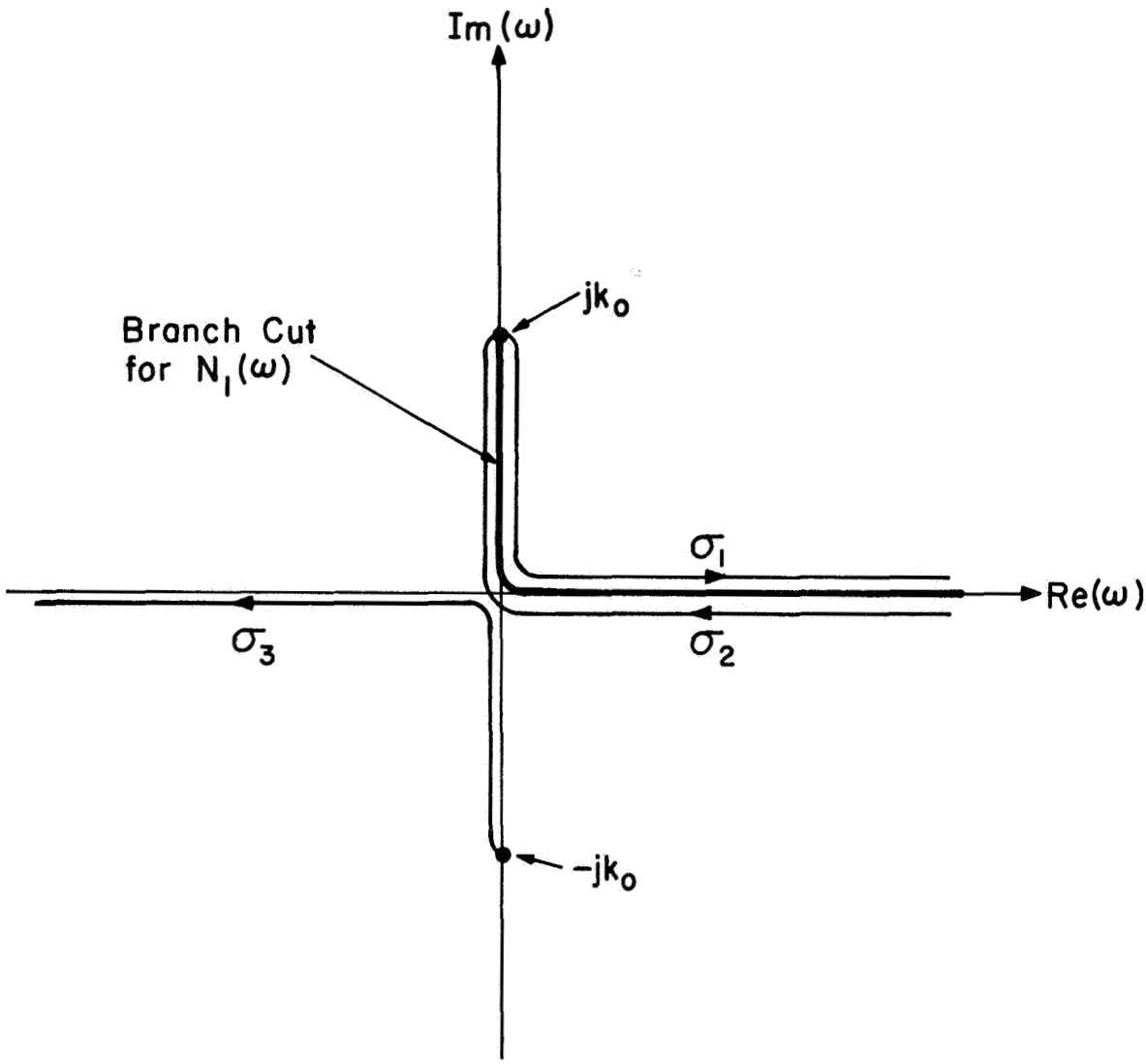

Figure 18. The branch cut for $N_1(\omega)$, the canonical form in circular geometry.

$$n_1(\omega) = \frac{\Pi(\omega,\eta)}{\Pi(\omega,\xi)} = \frac{\prod_{s=1}^{\infty}\left(1 - \frac{\omega}{\sqrt{\gamma_s^2-k_o^2}}\right) \exp\left(\frac{\omega}{\sqrt{\gamma_s^2-k_o^2}}\right)}{\prod_{s=1}^{\infty}\left(1 - \frac{\omega}{\sqrt{\alpha_s^2-k_o^2}}\right) \exp\left(\frac{\omega}{\sqrt{\alpha_s^2-k_o^2}}\right)} \tag{4.5}$$

The values of γ_s and α_s employed in (4.5) are given by the zeros of the characteristic equations for regions C and E respectively (cf. Figure 17)

$$J_o(\gamma_s b) = 0 \tag{4.6}$$

$$J_o(\alpha_s b)\, N_o(\alpha_s a) - N_o(\alpha_s b)\, J_o(\alpha_s a) = 0 \quad . \tag{4.7}$$

Before taking the above indicated limit, we give two standard reflection formulas

$$\Pi(\omega,\eta)\ \Pi(-\omega,\eta) = \frac{\prod_{s=1}^{\infty}\left[1 - \left(\frac{\alpha}{\gamma_s}\right)^2\right]}{\prod_{s=1}^{\infty}\left[1 - \left(\frac{k_o}{\gamma_s}\right)^2\right]} =$$

$$\frac{J_o(\alpha b)\, N_o(\alpha a) - N_o(\alpha b)\, J_o(\alpha a)}{J_o(k_o b)\, N_o(k_o a) - N_o(k_o b)\, J_o(k_o a)} \tag{4.8}$$

and

$$\Pi(\omega,\xi)\ \Pi(-\omega,\xi) = \frac{\prod_{s=1}^{\infty}\left[1 - \left(\frac{\alpha}{\alpha_s}\right)^2\right]}{\prod_{s=1}^{\infty}\left[1 - \left(\frac{k_o}{\alpha_s}\right)^2\right]} = \frac{J_o(\alpha a)}{J_o(k_o a)} \quad , \tag{4.9}$$

where $\alpha = \sqrt{\omega^2+k_o^2}$. Substituting (4.8), and (4.9) into the product $[n_1(\omega)\ n_1(-\omega)]$ yields

$$[n_1(\omega)\ n_1(-\omega)] = \frac{J_o(\alpha b)\left[\frac{N_o(\alpha a)}{J_o(\alpha a)}\right] - N_o(\alpha b)}{J_o(k_o b)\left[\frac{N_o(k_o a)}{J_o(k_o a)}\right] - N_o(k_o b)} \tag{4.10}$$

In the reflection relationships (4.8) and (4.9), we have employed the standard infinite product expansions for the appropriate Bessel functions (Abramowitz and Stegen, 1964). Our aim is to find the relationship corresponding to (4.10) for the open-region case. To this end, we let $a \to \infty$ in (4.10) and obtain

$$N_1(\omega)\, N_1(-\omega) = - \frac{N_o^{(1)}(\alpha b)}{N_o^{(2)}(k_o b)} \quad , \tag{4.11}$$

where $N_o^{(1)}$ and $N_o^{(2)}$ are Hankel functions of order zero.

Equation (4.11) is quite useful in numerical calculations. The function N_1 must be known both on paths σ_1 and its reflection σ_3, shown in Figure 18. With the aid of this reflection formula (4.11), we need only numerically calculate $N(\omega|_{\sigma_3})$ from the integral (4.4), and obtain $N(\omega|_{\sigma_1})$ directly from (4.11). This process yields a fifty-percent savings in integration time. Also, it is to our advantage to refrain from evaluating $N(\omega|_{\sigma_1})$ directly from the integral (4.4), due to the logarithmic singularity of the integrand when ω is on the path σ_1.

A second relationship involving the function $N_1(\omega)$ relates the function values on each side of the branch singularity. Such a relationship must be known when employing the function-theoretic technique. Evaluating (4.11) for ω on each side of the branch singularity, and by eliminating the common factor $N(-\omega|_{\sigma_3})$, we obtain

$$N_1(\omega|_{\sigma_2}) = N_1(\omega|_{\sigma_1}) \left[- \frac{N_o^{(2)}(\alpha b)}{N_o^{(1)}(\alpha b)} \right] \quad , \tag{4.12}$$

where the paths σ_1 and σ_2 are shown in Figure 18. For large values of

ω, (4.12) has the asymptotic representation

$$\lim_{\omega\to\infty}\left[\frac{N_1(\omega|_{\sigma_2})}{N_1(\omega|_{\sigma_1})}\right] = e^{-j(2\sqrt{\omega^2+k_o^2}\ b + \pi/2)} \quad . \tag{4.13}$$

The corresponding relationship for parallel-plate geometry is given by

$$\frac{\overline{N}_1(\omega|_{\sigma_2})}{\overline{N}_1(\omega|_{\sigma_1})} = e^{-j2\sqrt{\omega^2+k_o^2}\ b} \quad . \tag{4.14}$$

Equations (4.13) and (4.14) show the close correspondence between the canonical function N_1 for circular geometry and $\overline{N}_1$ for parallel-plane geometry in the asymptotic sense.

5. NUMERICAL RESULTS FOR PARALLEL-PLATE GUIDE WITH SLAB

Early attempts to solve the auxiliary integral equation (2.77) for $T(\omega|_{\sigma_1'})$ were carried out by employing an iterative technique. The term $(z|_{\sigma_1'} - \beta_p)^{-1}$ was substituted as a first approximation to T(z) in (2.77). The resulting numerical integration yielded a second order approximation. Subsequently, an n-th approximation was obtained by iteration of the (n-1)-th approximation. In general, it was found that for values of b and t which were of the same order of magnitude as the free-space wavelength Λ_0, the iterative method yielded a rapidly converging sequence of functions, i.e., only three or four iterations were required to give a solution which differed by less than one percent from the preceeding iterated result. However, when b and t were large compared to Λ_0, rapid divergence of the iterated result was encountered. In both the convergent and divergent cases, a plot of the logarithm of the magnitude of the iterated function for any fixed point on the path σ_1' against the number of the iteration, yielded a straight line. Even the logarithm of the function values for the first and second iterations lay on that line, indicating that the spectrum of eigenvalues of the truncated auxiliary integral equation was of a special character. The character is that there exists one eigenvalue, dominant in modulus over all the others in the spectrum. The dominant character of this eigenvalue may be used to advantage in the construction of a solution for the divergent case. However, for divergent and slowly convergent cases, matrix inversion was employed instead. It was found that the computation time required to invert a 50 x 50 complex matrix was comparable to ten iterations.

Some numerical solutions to the problem shown in Figure 1 were obtained using a high speed digital computer, viz., the IBM 360/75. In order to illustrate the effect of varying each of the physical parameters, the results are divided into the following categories: (1) variation in b, the waveguide half-width, (2) variation in ℓ, the slab-aperture separation, (3) variation in 2t, the slab thickness, and (4) variation in κ, the relative permittivity of the slab.

It was indicated in Section 2.6.2 that the number of nulls in the forward pattern is dependent on the waveguide half-width or in other words, equivalently dependent on the number of propagating guide-modes. Figures 19a through 19d show the radiation patterns for four different values of half-width. The values of b were chosen so that an additional mode propagates in subsequent figure(s), beginning with one in 19a and four in 19d. In each case, the incident mode was TEM, and this is the case for all results in this paper. Each pattern is normalized to unity in the broadside direction. Table 1 illustrates the distribution of power scattered into the various regions with the incident guide mode having unit power. The various values of scattered power have been renormalized after computation in order that their sum is unity. However, the total scattered power before renormalization was found to be within four percent of unity in nearly all cases and occasionally not more than twelve percent. By increasing the number of sample points or the point of truncation in the numerical integration of the auxiliary integral equation, accuracy may be increased at the expense of computation time. However, it was found that such an increase in accuracy had very little effect on the "shape" of the radiation pattern, and only affected the distribution of scattered power. Typical machine-time for a single solution was about half-a-minute.

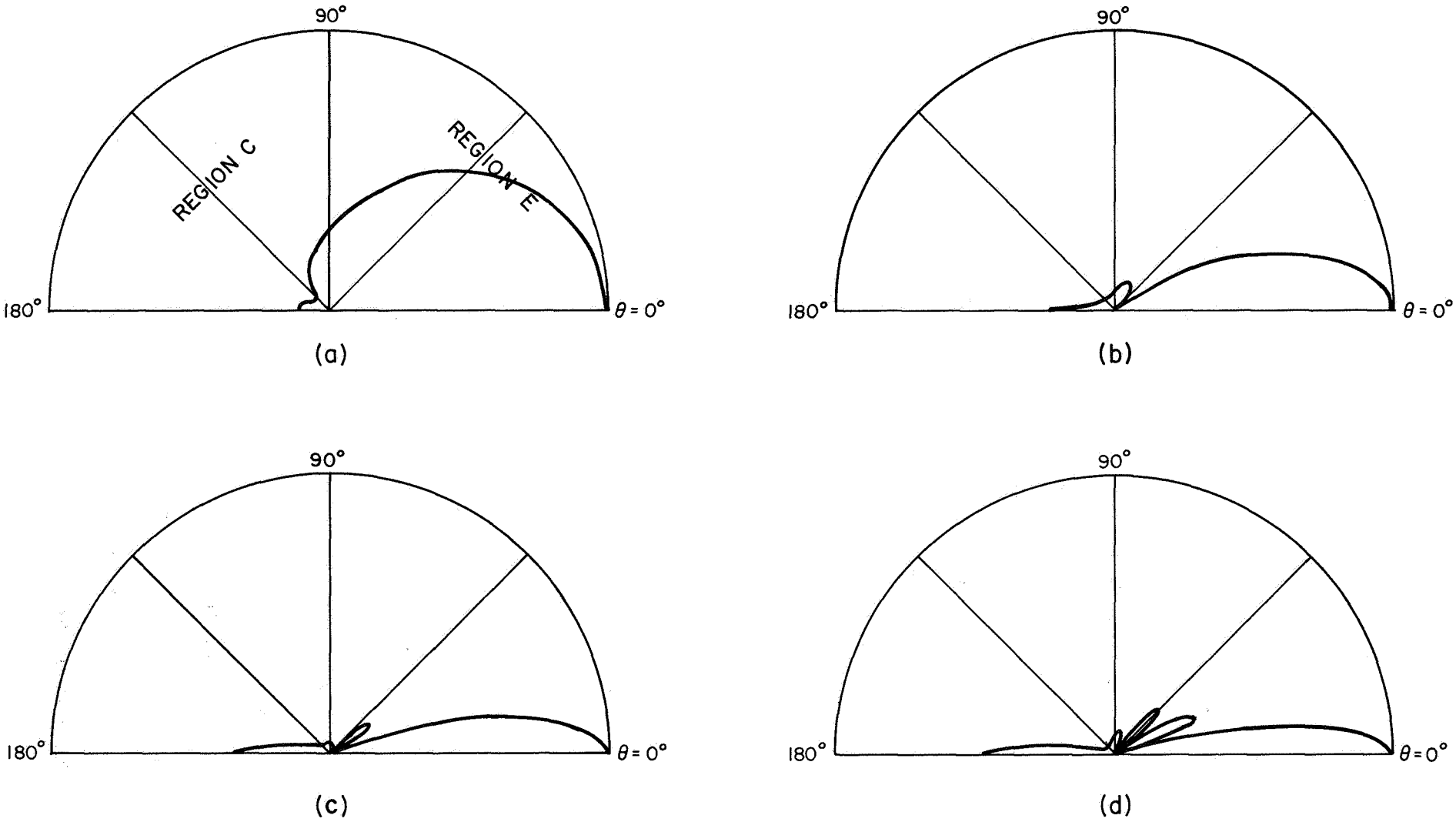

Figure 19. The radiation pattern for $k_o = 1$, $\kappa = 2$, $2t = \Lambda_o/2$, $\ell = 0$, and various values of b, the waveguide half-width. (a) $b = \Lambda_o/4$, (b) $b = 3\Lambda_o/4$, (c) $b = 5\Lambda_o/4$, and (d) $b = 7\Lambda_o/4$. The free-space wavelength is Λ_o.

Table 1. The scattered power for several values of b, the waveguide half-width. $k_o = 1$, $k = 2$, $2t = \Lambda_o/2$, $\ell = 0$. The free-space wavelength is Λ_o.

b	P_{B_o} WATTS TEM	P_{B_1} WATTS TM_{10}	P_{B_2} WATTS TM_{20}	P_{B_3} WATTS TM_{30}	P_B WATTS TOTAL	P_E WATTS	P_C WATTS	P_{A_o} WATTS TM_o	P_{A_1} WATTS TM_1	P_A WATTS TOTAL
$\frac{\Lambda_o}{4}$	8.704E-2*	--	--	--	8.704E-2	8.445E-1	3.213E-2	4.475E-9	3.627E-2	3.627E-2
$\frac{3\Lambda_o}{4}$	2.896E-2	9.400E-3	--	--	3.835E-2	9.268E-1	3.474E-2	7.763E-10	1.724E-4	1.724E-4
$\frac{5\Lambda_o}{4}$	2.611E-2	9.034E-3	1.299E-3	--	3.644E-2	9.020E-1	6.447E-2	2.375E-10	1.564E-7	1.566E-7
$\frac{7\Lambda_o}{4}$	2.390E-2	2.053E-2	1.924E-3	2.883E-3	4.923E-2	8.266E-1	1.242E-1	1.138E-9	4.270E-7	4.281E-7

* The notation y.yyyEz means y.yyy x 10^z.

As indicated in Figure 19 and Table 1, the main lobe of the pattern narrows as the guide half-width is increased with little affect on the forward radiated power P_E. This result would also occur in the absence of the dielectric slab. An increase in b has a detrimental effect on the efficiency of surface mode excitation. Table 1 indicates that as the guide aperture is widened, the total power P_A in the surface modes is decreased.

The effect of changing the distance between the guide aperture and slab is next considered. Figures 20a through 20f show the radiation patterns when the distance ℓ is varied from zero to Λ_0. As indicated in Section 2.6.2, the forward pattern is nearly independent of ℓ, while its shape depends on the transmission factor $\overline{T}$. This independence of ℓ is illustrated by the close similarity of the forward patterns of Figures 20a through 20f. The forward radiated power P_E, shown in Table 2, is also nearly independent of ℓ.

The dependence of the pattern in the backward direction on ℓ is not so simple, due to the phase relationship between the direct and reflected fields in the composite field representation discussed in Section 2.6.2. Table 2 compares the distribution of scattered power for various values of ℓ and shows that the excitation of surface modes becomes increasingly difficult as the slab is moved away from the waveguide aperture.

In varying the slab thickness 2t, the pattern and scattered power have been obtained for various fractions of Λ_0, the free-space wavelength, instead of the wavelength within the slab. Figures 21a through 21f show the radiation patterns when the slab thickness varies from zero to Λ_0.

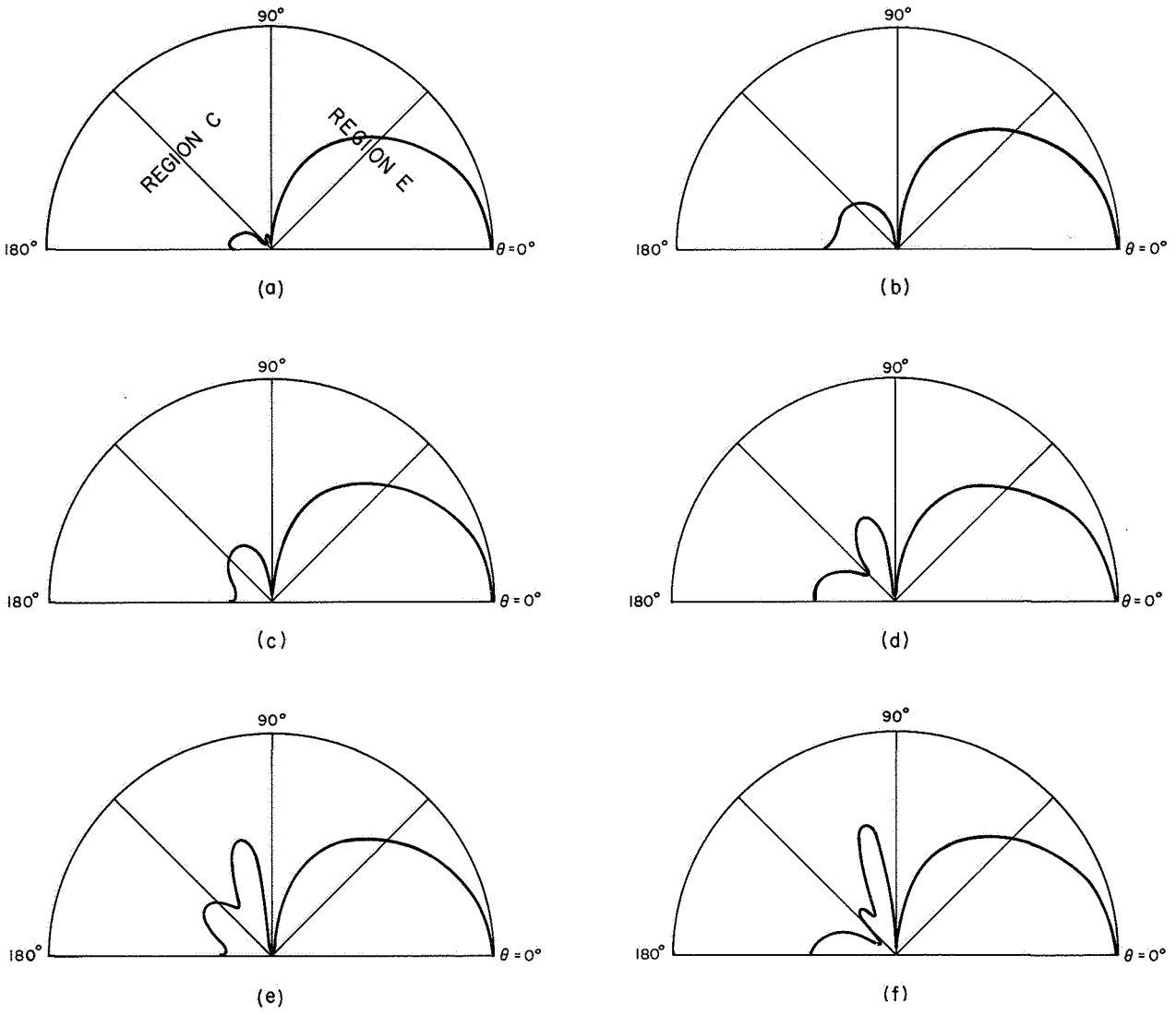

Figure 20. The radiation pattern for $k_o = 1$, $\kappa = 2$, $b = \Lambda_o/4$, $2t = \Lambda_o/4$, and various values of ℓ, the aperture-slab separation. (a) $\ell = 0$, (b) $\ell = \Lambda_o/8$, (c) $\ell = \Lambda_o/4$, (d) $\ell = \Lambda_o/2$, (e) $\ell = 3\Lambda_o/4$, and (f) $\ell = \Lambda_o$. The free-space wavelength is Λ_o.

Table 2. The scattered power for various values of ℓ, the aperture-slab separation $k_o = 1$, $\kappa = 2$, $b = \Lambda_o/4$, and $2t = \Lambda_o/4$. The free-space wavelength is Λ_o.

ℓ	P_{B_o} WATTS TEM	P_E WATTS	P_C WATTS	P_{A_o} WATTS TM_o
0	5.284E-2	7.040E-1	1.856E-2	2.247E-1
$\frac{\Lambda_o}{8}$	2.017E-3	7.254E-1	8.257E-2	1.898E-1
$\frac{\Lambda_o}{4}$	5.322E-2	7.528E-1	7.100E-2	1.228E-1
$\frac{\Lambda_o}{2}$	5.737E-2	7.764E-1	1.335E-1	3.280E-2
$\frac{3\Lambda_o}{4}$	3.931E-2	7.735E-1	1.777E-1	9.562E-3
Λ_o	5.211E-2	7.851E-1	1.601E-1	2.709E-3

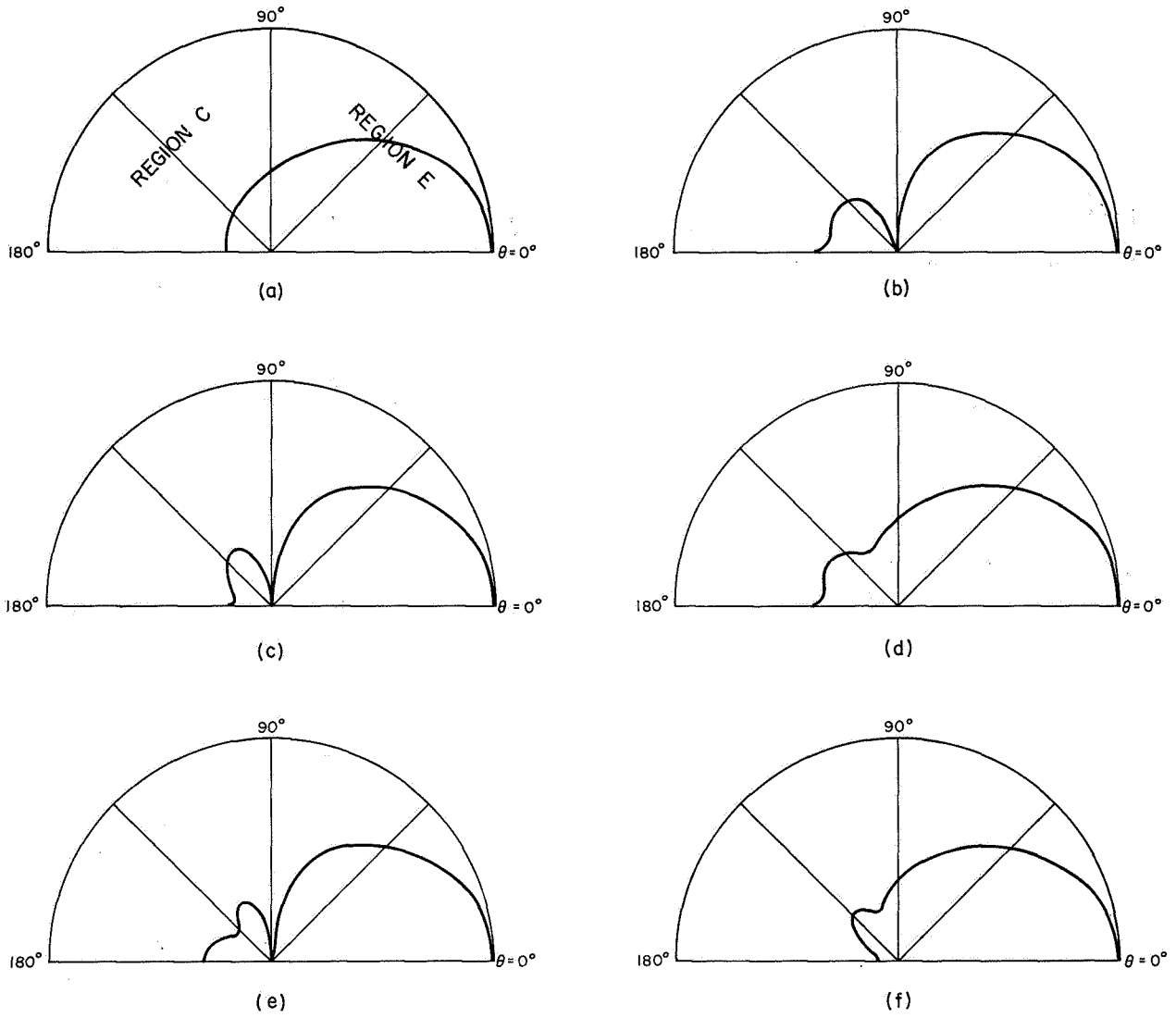

Figure 21. The radiation pattern for $k_o = 1$, $\kappa = 2$, $b = \Lambda_o/4$, $\ell = \Lambda_o/4$, and various values of $2t$, the slab thickness. (a) $2t = 0$, (b) $2t = \Lambda_o/8$, (c) $2t = \Lambda_o/4$, (d) $2t = \Lambda_o/2$, (e) $2t = 3\Lambda_o/4$, and (f) $2t = \Lambda_o$. The free-space wavelength is Λ_o.

Table 3. The scattered power for various values of 2t, the slab width, given as fractions of Λ_o, the free-space wavelength. $k_o = 1$, $\kappa = 2$, $b = \Lambda_o/4$, $\ell = \Lambda_o/4$.

2t	P_{B_0} watts TEM	P_E watts	P_C watts	P_{A_0} watts TM_0	P_{A_1} watts TM_1	P_A watts TOTAL
0	4.319E-2	8.547E-1	1.021E-1	—	—	—
$\frac{\Lambda_o}{8}$	1.545E-2	7.802E-1	1.075E-1	9.714E-2	—	9.714E-2
$\frac{\Lambda_o}{4}$	5.322E-2	7.528E-1	7.099E-2	1.228E-1	—	1.228E-1
$\frac{\Lambda_o}{2}$	2.231E-2	8.192E-1	1.589E-1	7.405E-9	4.659E-3	4.659E-3
$\frac{3\Lambda_o}{4}$	3.213E-2	8.523E-1	9.478E-2	1.918E-2	1.660E-3	2.084E-2
Λ_o	4.706E-2	8.477E-1	9.421E-2	1.034E-2	6.800E-4	1.102E-2

An interesting behavior of the total surface mode power P_A is observed. As the slab thickness is increased, the amount of power carried by the surface modes increases. However, when the slab is sufficiently thick, allowing another mode to propagate, the total power P_A decreases. A further increase in slab thickness again increases the surface mode power until another mode begins to propagate.

Numerical results for various values of slab permittivity are shown in Figures 22a through 21e. radiation patterns are shown only for positive values of κ, since little power is radiated when the slab is a plasma and when the aperture-slab separation ℓ is zero. The effect of an increase in κ is to broaden the forward lobe of the pattern. This effect is accompanied by a decrease in the forward radiated power P_E, indicated in Table 4. Also shown in Table 4 are several cases for plasma slabs. When $\kappa < 0$, a large fraction of the power is reflected back into the waveguide, as indicated in the column headed P_B. For large negative values of κ, both the forward and backward radiated power is reduced; however, there is a greater fraction of power leaking around the guide edge into region C than is radiated through the slab into region E. This is the case when $\ell = 0$. When the plasma slab is not directly against the guide aperture, an appreciable amount of power will be radiated into the backward region.

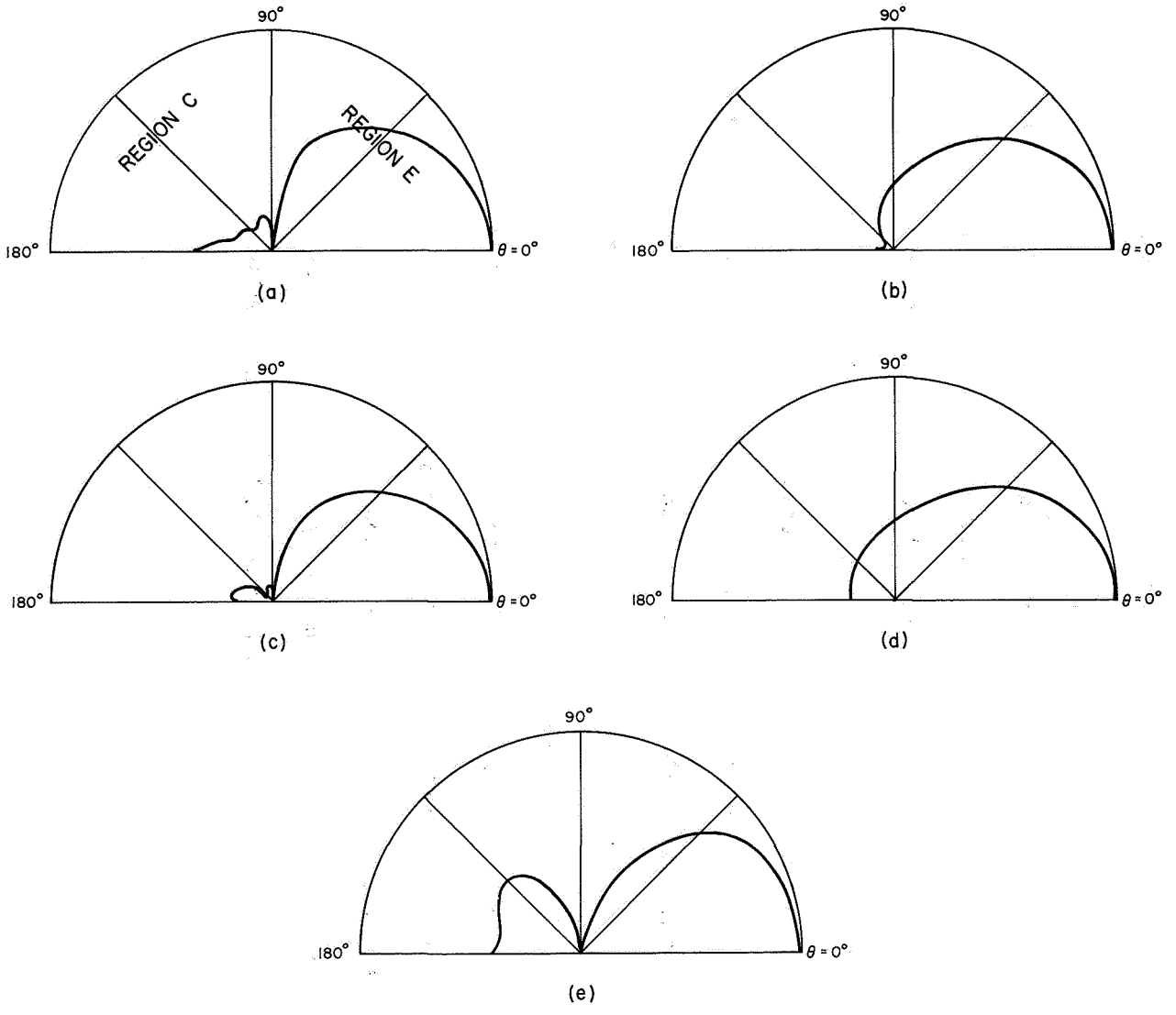

Figure 22. The radiation pattern for $k_o = 1$, $b = \Lambda_o/4$, $2t = \Lambda_o/4$, $\ell = 0$, and various values of κ, the relative dielectric constant of the slab. (a) $\kappa = 10$, (b) $\kappa = 5$, (c) $\kappa = 2$, (d) $\kappa = 1$, and (e) $\kappa = 0.5$. The free space wavelength is Λ_o.

Table 4. The scattered power for various values of κ, the relative dielectric constant of the slab. $k_o = 1$, $b = \Lambda_o/4$, $2t = \Lambda_o/4$, $\ell = 0$. The free-space wavelength is Λ_o.

κ	P_{B_o} watts TEM	P_E watts	P_C watts	P_{A_o} watts TM_0	P_{A_1} watts TM_1	P_A watts TOTAL
10	5.367E-1	4.148E-1	2.166E-2	1.243E-3	2.546E-2	2.670E-2
5	7.608E-2	8.546E-1	2.813E-2	5.566E-10	4.893E-2	4.893E-2
2	5.284E-2	7.050E-1	1.856E-2	2.247E-1	—	2.247E-1
1	4.320E-2	8.547E-1	1.021E-1	—	—	—
0.5	9.688E-2	7.153E-1	1.875E-1	—	—	—
0	9.709E-1	1.367E-2	1.541E-2	—	—	—
-0.5	7.734E-1	1.826E-1	4.395E-2	—	—	—
-2	9.001E-1	4.739E-2	5.259E-2	—	—	—
-5	9.624E-1	2.379E-3	3.517E-2	—	—	—
-10	9.711E-1	8.320E-5	2.878E-2	—	—	—

6. CONCLUSIONS

The present solution for radiation from an open-ended parallel-plate waveguide through a dielectric or plasma slab lends itself to a numerically accurate and rapid solution. Typically, the function-theoretic technique and its subsequent extensions and modifications (hereafter called MFT) have several distinct advantages over other methods. compared with some variational techniques for the same problem, the MFT yields at least the most useful information, viz., waveguide reflection coefficients. However, with little additional but straightforward computations, all of the scattered fields can be determined. Formulation in terms of the characteristic modes for each region in the MFT leads to a simple mode matching procedure. The process of continuing the incident waveguide field into the open-region, as is the case when the Weiner-Hopf technique is employed, is not in line with a physical understanding of the problem. Finally, the correct edge condition is automatically satisfied, since a priori information of the asymptotic behavior of the fields in the neighborhood of the waveguide edge is incorporated in the MFT. In contrast, the satisfaction of this important condition is difficult - if not impossible - to show when other methods are employed. For example, Mittra (1963) demonstrated that satisfaction of the edge condition in the solution of a doubly-infinite set of matrix equations relating to the closed-region waveguide bifurcation problem, was strongly dependent upon the way in which the number of equations was determined in the truncation procedure.

Application of the MFT to waveguide problems other than the basic parallel-plate geometry, requires only a straightforward extension of

the method employed for the simpler geometry. The solutions for circular guides with rotationally independent fields are easily obtained, and they possess all of the desirable characteristics of parallel-plate geometry. Also the MFT is easily extended to geometries containing layered media in the open-regions. Such layered problems are encountered in diagnostics of laboratory plasmas, where a bulk plasma is surrounded by an ion sheath and glass envelope.

Other problems which are easily attacked by the MFT include: (1) The flanged waveguide; (2) radiation from an open-ended waveguide onto a reflecting screen; and (3) a flanged guide radiating through a plasma or dielectric slab. In fact, most open-ended waveguide problems in which the geometry is uniform in the transverse direction but longitudinally non-uniform can be formulated and solved by the MFT.

BIBLIOGRAPHY

Abramowitz, M. and Stegun, Irene. (1964), Handbook of Mathematical Functions. U. S. Department of Commerce National Bureau of Standards Applied Mathematics Series, 85.

Bateman, H. (1954), Tables of Integral Transforms. Vol. 2, McGraw-Hill.

Bates, C. P. and Mittra, R. (1967), "Waveguide Excitation of Dielectric and Plasma Slabs," Radio Sci. J. Res. NBS., Vol. 3 (New Series), No. 4, 251-66.

Berz, F. (1951), "Reflection and Refraction of Microwaves at a Set of Parallel Metallic Plates," Proc. I.E.E. (London) 98, Pt. 3, 47-55.

Collin, R. E. (1960), Field Theory of Guided Waves. McGraw-Hill.

Hurd, R. A. and Gruenberg, H. (1954), "H-Plane Bifurcation of Rectangular Waveguides," Canadian J. Physics, 32, 694-701.

Jolly, L. B. W. (1961), Summation of Series. Dover.

Jordan, E. C. (1950), Electromagnetic Waves and Radiating Systems. Prentice-Hall.

Meixner, J. (1954), "The Behavior of Electromagnetic Fields at Edges," N.Y. Univ. Inst. Math. Sci. Research Report - EM-72, Dec.

Mittra, R. (1963), "Relative Convergence of the Solution of a Doubly Infinite Set of Equations," J. Res. NBS., 67D, 245-254.

Mittra, R. and Bates, C. P. (1965), "An Alternative Approach to the Solution of a Class of Weiner-Hopf and Related Problems," Proceedings of the Electromagnetic Wave Theory Symposium, Delf, The Netherlands, Sept.

Mittra, R., Lee, S. W., and Vanblaricum, G. F. (1968), "A Modified Residue Calculus Technique," Univ. of Ill. Antenna Lab. Report No. 68-1, Univ. of Ill., Urbana, Ill.

Muskhelishvili, N. I. (1953), Singular Integral Equations. P. Noordhoff N. V. - Groningen-Holland.

Noble, B. (1958), Methods Based on the Weiner-Hopf Technique. Pergamon Press.

Whitehead, E. A. N. (1951), "The Theory of Parallel-Plate Media for Microwave Lenses," Proc. I.E.E. (London) 98, Pt. 3, 133-40.

APPENDIX

ESTIMATION OF THE TRUNCATION ERROR FOR INFINITE PRODUCT EXPANSIONS

In the numerical solution of problems via the function-theoretic technique and its subsequent modifications, one is required to evaluate infinite product expansions of the following form:

$$\Pi(\omega,\beta) = \prod_{s=1}^{\infty} \left[1 - \frac{\omega}{\beta}\right] \exp(\omega/\beta_s) \qquad \text{(A1)}$$

where $\beta_s = \sqrt{\left(\frac{s\pi}{b}\right)^2 - k_o^2}$, k_o and b are constants described elsewhere, and ω is the function variable. To an end of evaluating (A1) in a truncated form, together with an estimate of the truncation error, we write

$$\Pi(\omega,\beta) = \left(\prod_{s=1}^{K} (1 - \omega/\beta_s) \exp(\omega/\beta_s) \right) \varepsilon_K \qquad \text{(A2)}$$

The expression for the truncation error ε_K is given by

$$\varepsilon_K = \exp\left[\sum_{s=K+1}^{\infty} [\ln(1 - \omega/\beta_s) + \omega/\beta_s] \right] \qquad \text{(A3)}$$

Expanding the logrithmic part of (A3) in a power series when $(K + 1)\ \pi/(2bk_o) > |\omega/k_o| > 1$, we obtain

$$\varepsilon_K = \exp\left\{ \sum_{\substack{s=K+1 \\ t=2}}^{\infty} \left[\frac{1}{t} \left(\frac{\omega}{\beta_s} \right)^t \right] \right\} . \qquad \text{(A4)}$$

Interchanging the indices of summation, i.e., summing on t first, together with the relationship

$$\left[\frac{b}{\pi(K-1)}\right]^t \left[\frac{K-1}{t-1}\right] = \int_{K+1}^{\infty} \left[\frac{b}{(s-2)\pi}\right]^t ds \geq \sum_{s=K+1}^{\infty} \left[\frac{1}{\beta_s}\right]^t \geq$$

$$\int_{K+1}^{\infty} \left[\frac{b}{s\pi}\right]^t ds = \left[\frac{b}{\pi(K+1)}\right]^t \left[\frac{K+1}{t-1}\right] , \qquad \text{(A5)}$$

which is valid for $(K+1) > \frac{1}{2}\left[\left(\frac{k_o b}{\pi}\right)^2 + 1\right]$, we obtain bounds for the truncation error for ω-real

$$\exp\left\{-(K-1)\sum_{t=2}^{\infty}\left[\frac{b\,\omega}{\pi(K-1)}\right]^t\left[\frac{1}{t(t-1)}\right]\right\} \leq \varepsilon_K \leq$$

$$\exp\left\{-(K+1)\sum_{t=2}^{\infty}\left[\frac{b\omega}{\pi(K+1)}\right]^t\left[\frac{1}{t(t-1)}\right]\right\}. \qquad \text{(A6)}$$

The summations in (A6) can be evaluated exactly (Jolly, 1961)

$$\sum_{t=2}^{\infty}\left[\frac{x^t}{t(t-1)}\right] = x + (1-x)\ln(1-x) \quad . \qquad \text{(A7)}$$

Substituting (A7) into (A6) and taking only the first term in the power series expansion of $\ln(1-x)$, we find that ε_K has the following asymptotic representation:

$$\varepsilon_K \cong \exp\left[-\frac{1}{2}\left(\frac{\omega b}{\pi}\right)^2\right] \quad , \qquad \text{(A8)}$$

when $K >> \frac{|\omega| b}{\pi}$.

Equation (A8) is found numerically to yield excellent results for $|\omega| < 10k_o$ and $K = 100$. To a first order approximation, the value of ε_K is the same for both $\pm\,\omega$. One may check the accuracy of (A1) as computed from (A2) by use of the following reflection formula in which the truncation error is cumulative:

$$\Pi(\omega,\beta)\ \Pi(-\omega,\beta) = \frac{k_o \sin(\alpha b)}{\alpha \sin(k_o b)} \quad , \tag{A9}$$

where $\alpha = \sqrt{k_o^2+\omega^2}$. We further note that in the solution of the auxiliary integral equation (cf. section 2.4), factors of the form $\Pi(\omega,\beta)/\Pi(-\omega,\beta)$ are encountered. Due to the even symmetry of the truncation error (A8), we see that in the above quotient of infinite product expansions, the truncation error is self-canceling.

Unclassified
Security Classification

DOCUMENT CONTROL DATA - R&D

(Security classification of title, body of abstract and indexing annotation must be entered when the overall report is classified)

1. ORIGINATING ACTIVITY (Corporate author)	2a. REPORT SECURITY CLASSIFICATION
University of Illinois, Urbana, Illinois 61801	Unclassified
	2b. GROUP

3. REPORT TITLE

RADIATION FROM AN OPEN-ENDED WAVEGUIDE INTO AN INHOMOGENEOUSLY FILLED SPACE

4. DESCRIPTIVE NOTES (Type of report and inclusive dates)

Scientific - Interim

5. AUTHOR(S) (Last name, first name, initial)

Kostelnicek, R. J. and Mittra, R.

6. REPORT DATE	7a. TOTAL NO. OF PAGES	7b. NO. OF REFS
July 1969	77	15

8a. CONTRACT OR GRANT NO.	9a. ORIGINATOR'S REPORT NUMBER(S)
NGR-14-005-009	Scientific Report No. 12
b. PROJECT AND TASK NO.	Antenna Laboratory Report No. 69-10
c.	9b. OTHER REPORT NO(S) (Any other numbers that may be assigned this report)
d.	

10. AVAILABILITY/LIMITATION NOTICES

11. SUPPLEMENTARY NOTES	12. SPONSORING MILITARY ACTIVITY

13. ABSTRACT

An analytic solution to the problem of radiation from an open-ended parallel-plate waveguide into a dielectric or plasma slab is obtained. The electromagnetic fields are formulated in terms of a discrete mode spectrum inside the waveguide and continuous mode spectra in the open regions. Mode matching at the waveguide aperture plane leads to a singular integral equation. A solution of this equation allows the determination of the fields throughout the whole of space. However, this equation is not solved directly, but instead, an auxiliary integral equation is formed from the original equation by employing the known exact solution of the canonical problem, viz., radiation from an open-ended waveguide into free-space. The auxiliary equation has the advantage that it may be solved exactly in an asymptotic sense. This asymptotic solution demonstrates that the correct edge condition is satisfied. Standard numerical techniques are employed, and results giving the fields and distribution of scattered power for a TEM incident mode are presented.

Solutions for other problems are also formulated, viz., the flanged waveguide and a guide radiating into a reflecting screen. These problems may also be solved when the geometry is circular. Furthermore, the edge condition is also shown to be satisfied in circular geometry.

DD FORM 1 JAN 64 1473

Unclassified
Security Classification

Unclassified
Security Classification

14. KEY WORDS	LINK A		LINK B		LINK C	
	ROLE	WT	ROLE	WT	ROLE	WT
Radiation Dielectric Singular Integral Equation Waveguide						

INSTRUCTIONS

1. ORIGINATING ACTIVITY: Enter the name and address of the contractor, subcontractor, grantee, Department of Defense activity or other organization *(corporate author)* issuing the report.

2*a*. REPORT SECURITY CLASSIFICATION: Enter the overall security classification of the report. Indicate whether "Restricted Data" is included. Marking is to be in accordance with appropriate security regulations.

2*b*. GROUP: Automatic downgrading is specified in DoD Directive 5200.10 and Armed Forces Industrial Manual. Enter the group number. Also, when applicable, show that optional markings have been used for Group 3 and Group 4 as authorized.

3. REPORT TITLE: Enter the complete report title in all capital letters. Titles in all cases should be unclassified. If a meaningful title cannot be selected without classification, show title classification in all capitals in parenthesis immediately following the title.

4. DESCRIPTIVE NOTES: If appropriate, enter the type of report, e.g., interim, progress, summary, annual, or final. Give the inclusive dates when a specific reporting period is covered.

5. AUTHOR(S): Enter the name(s) of author(s) as shown on or in the report. Enter last name, first name, middle initial. If military, show rank and branch of service. The name of the principal author is an absolute minimum requirement.

6. REPORT DATE: Enter the date of the report as day, month, year, or month, year. If more than one date appears on the report, use date of publication.

7*a*. TOTAL NUMBER OF PAGES: The total page count should follow normal pagination procedures, i.e., enter the number of pages containing information.

7*b*. NUMBER OF REFERENCES: Enter the total number of references cited in the report.

8*a*. CONTRACT OR GRANT NUMBER: If appropriate, enter the applicable number of the contract or grant under which the report was written.

8*b*, 8*c*, & 8*d*. PROJECT NUMBER: Enter the appropriate military department identification, such as project number, subproject number, system numbers, task number, etc.

9*a*. ORIGINATOR'S REPORT NUMBER(S): Enter the official report number by which the document will be identified and controlled by the originating activity. This number must be unique to this report.

9*b*. OTHER REPORT NUMBER(S): If the report has been assigned any other report numbers *(either by the originator or by the sponsor)*, also enter this number(s).

10. AVAILABILITY/LIMITATION NOTICES: Enter any limitations on further dissemination of the report, other than those imposed by security classification, using standard statements such as:

(1) "Qualified requesters may obtain copies of this report from DDC."
(2) "Foreign announcement and dissemination of this report by DDC is not authorized."
(3) "U. S. Government agencies may obtain copies of this report directly from DDC. Other qualified DDC users shall request through _____."
(4) "U. S. military agencies may obtain copies of this report directly from DDC. Other qualified users shall request through _____."
(5) "All distribution of this report is controlled. Qualified DDC users shall request through _____."

If the report has been furnished to the Office of Technical Services, Department of Commerce, for sale to the public, indicate this fact and enter the price, if known.

11. SUPPLEMENTARY NOTES: Use for additional explanatory notes.

12. SPONSORING MILITARY ACTIVITY: Enter the name of the departmental project office or laboratory sponsoring *(paying for)* the research and development. Include address.

13. ABSTRACT: Enter an abstract giving a brief and factual summary of the document indicative of the report, even though it may also appear elsewhere in the body of the technical report. If additional space is required, a continuation sheet shall be attached.

It is highly desirable that the abstract of classified reports be unclassified. Each paragraph of the abstract shall end with an indication of the military security classification of the information in the paragraph, represented as *(TS), (S), (C), or (U).*

There is no limitation on the length of the abstract. However, the suggested length is from 150 to 225 words.

14. KEY WORDS: Key words are technically meaningful terms or short phrases that characterize a report and may be used as index entries for cataloging the report. Key words must be selected so that no security classification is required. Identifiers, such as equipment model designation, trade name, military project code name, geographic location, may be used as key words but will be followed by an indication of technical context. The assignment of links, rules, and weights is optional.

Unclassified
Security Classification